Electronic Supplementary Information

Development of hydrogen-bonded dimer-type photoluminescent liquid crystals of fluorinated tolanecarboxylic acid

Shigeyuki Yamada [1,*], Mitsuki Kataoka [1], Keigo Yoshida [1], Masakazu Nagata [2,3], Tomohiro Agou [2], Hiroki Fukumoto [2], ant Tsutomu Konno [1]

[1] Faculty of Molecular Chemistry and Engineering, Kyoto Institute of Technology, Matsugasaki, Sakyo-ku, Kyoto 606-8585, Japan

[2] Department of Quantum Beam Science, Graduate School of Science and Engineering, Ibaraki University, 4-12-1 Nakanarusawa, Hitachi, Ibaraki 316-8511, Japan

[3] Present address: Organic Materials Chemistry Group, Sagami Chemical Research Institute, Hayakawa 2743-1, Ayase, Kanagawa 252-1193, Japan

* Correspondence: syamada@kit.ac.jp (S.Y.); Tel: +81-75-724-7517

Table of Contents

NMR spectrum

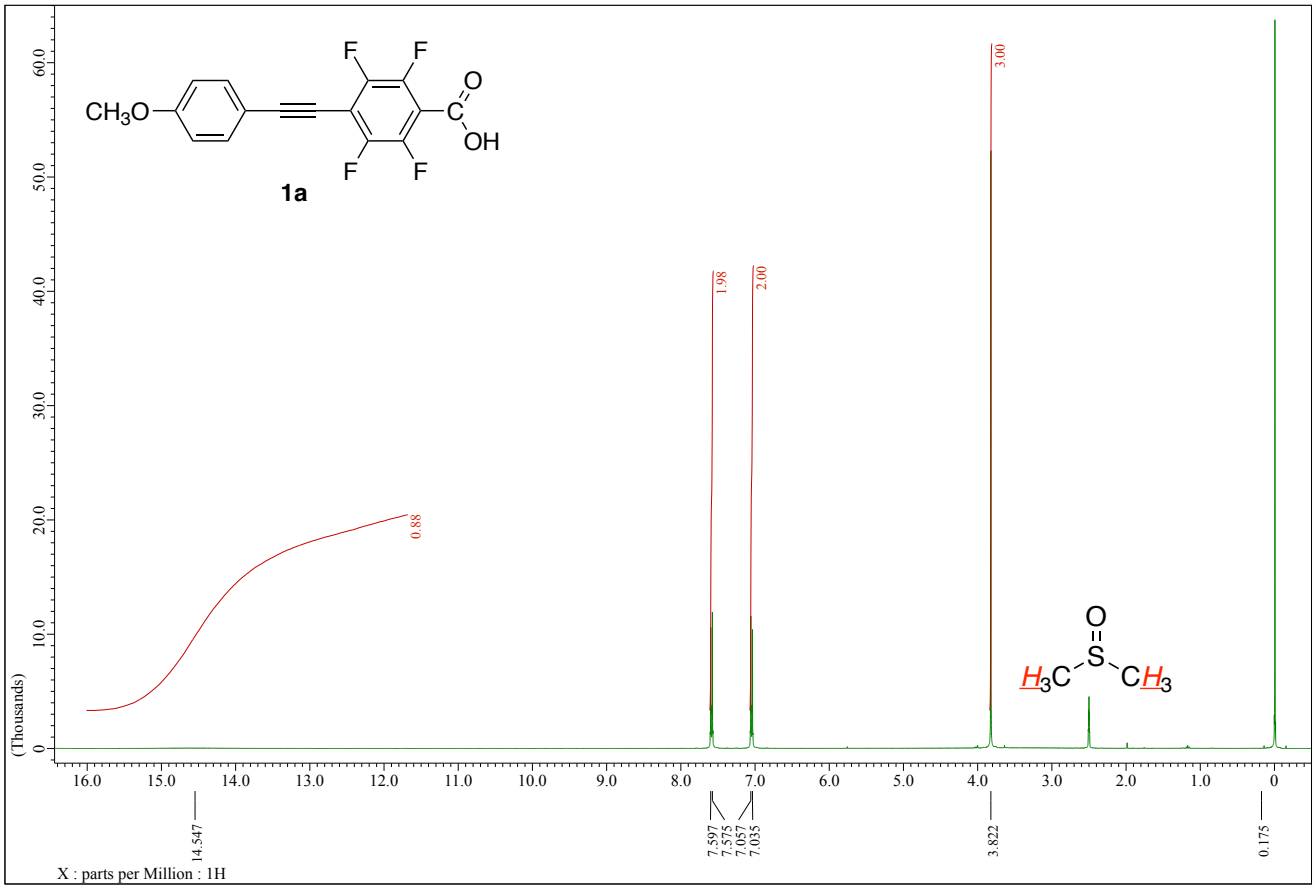

Figure S1. ^{1}H NMR spectrum of **1a** (DMSO-d_6, 400 MHz).

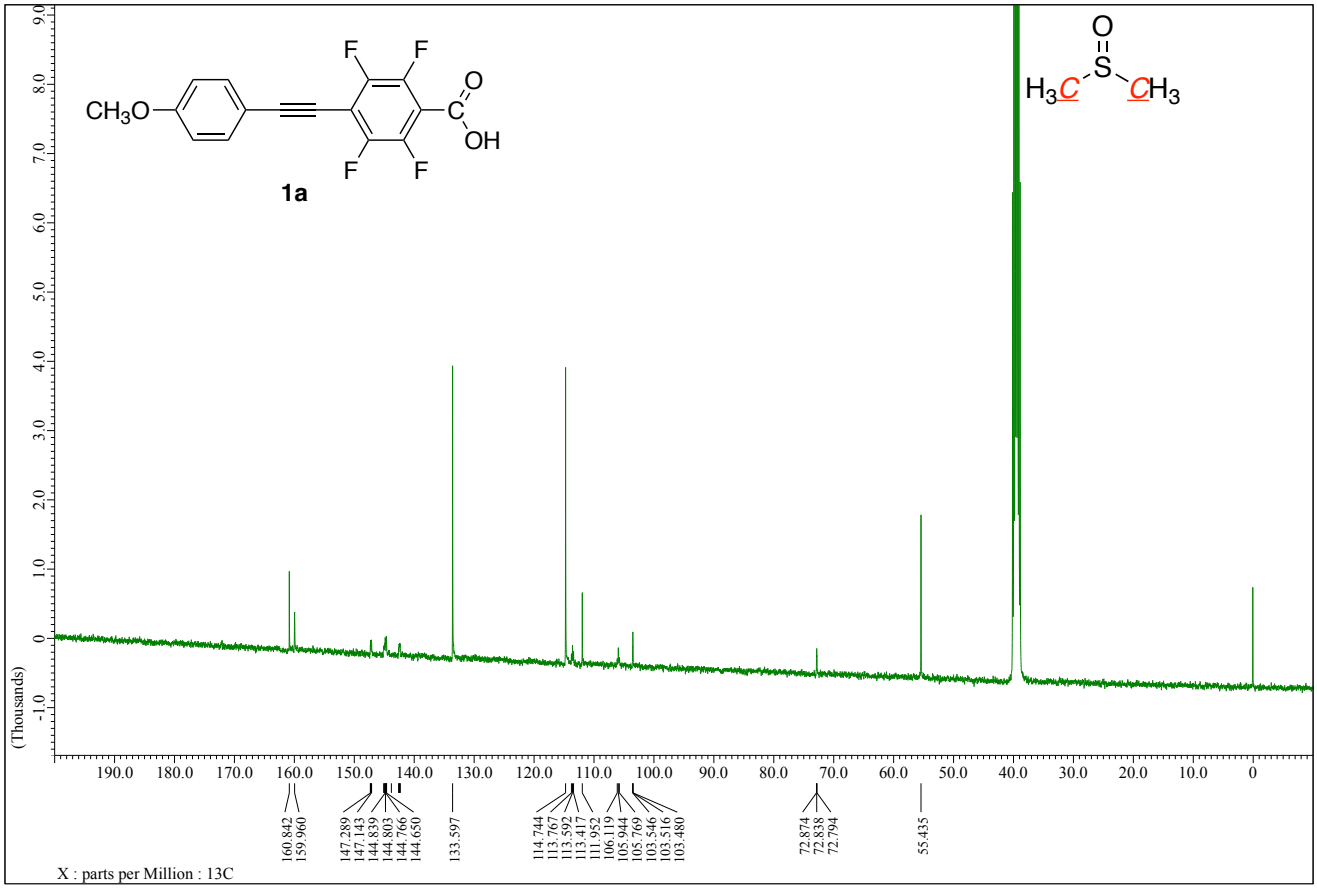

Figure S2. ^{13}C NMR spectrum of **1a** (DMSO-d_6, 100 MHz).

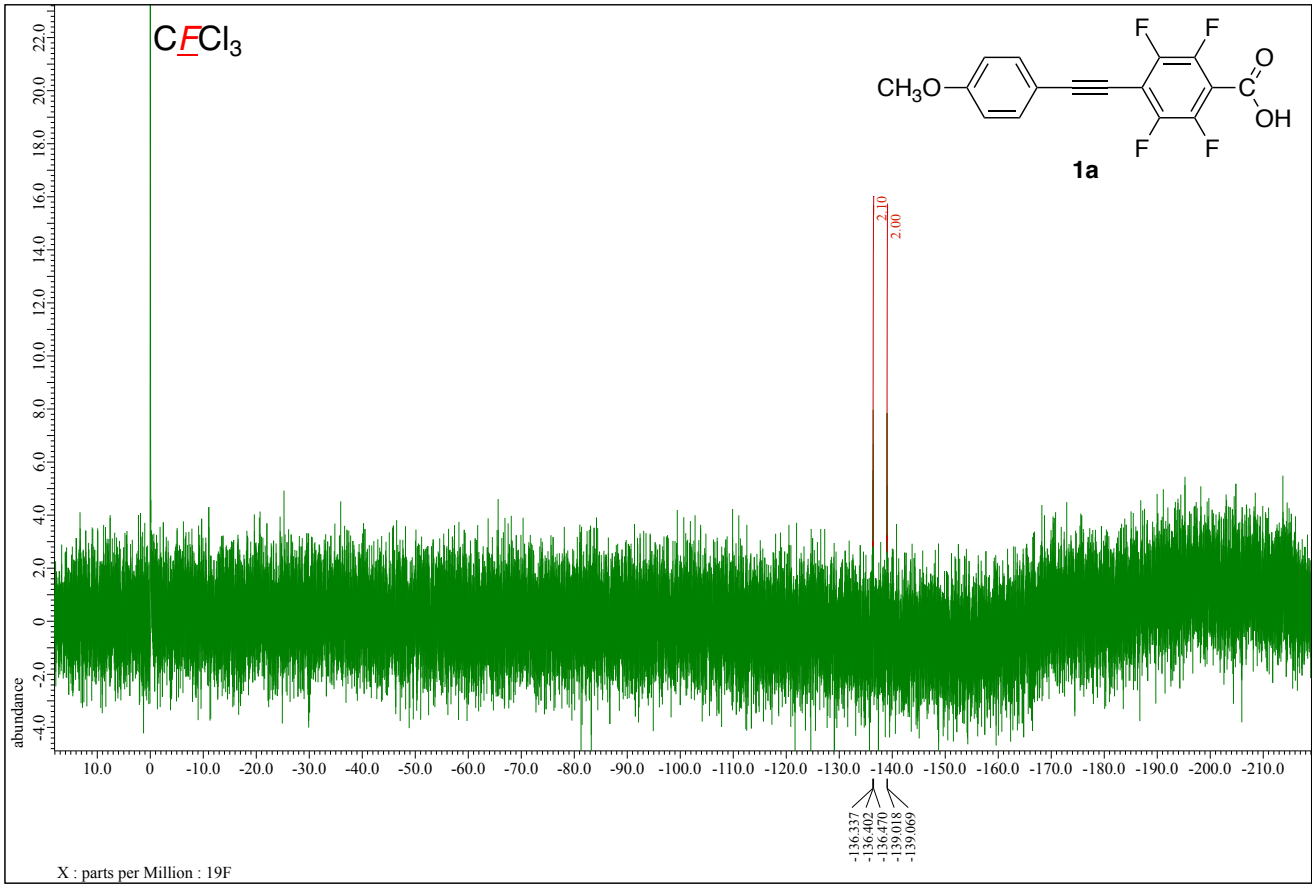

Figure S3. ^{19}F NMR spectrum of **1a** (DMSO-d_6, $CFCl_3$, 376 MHz).

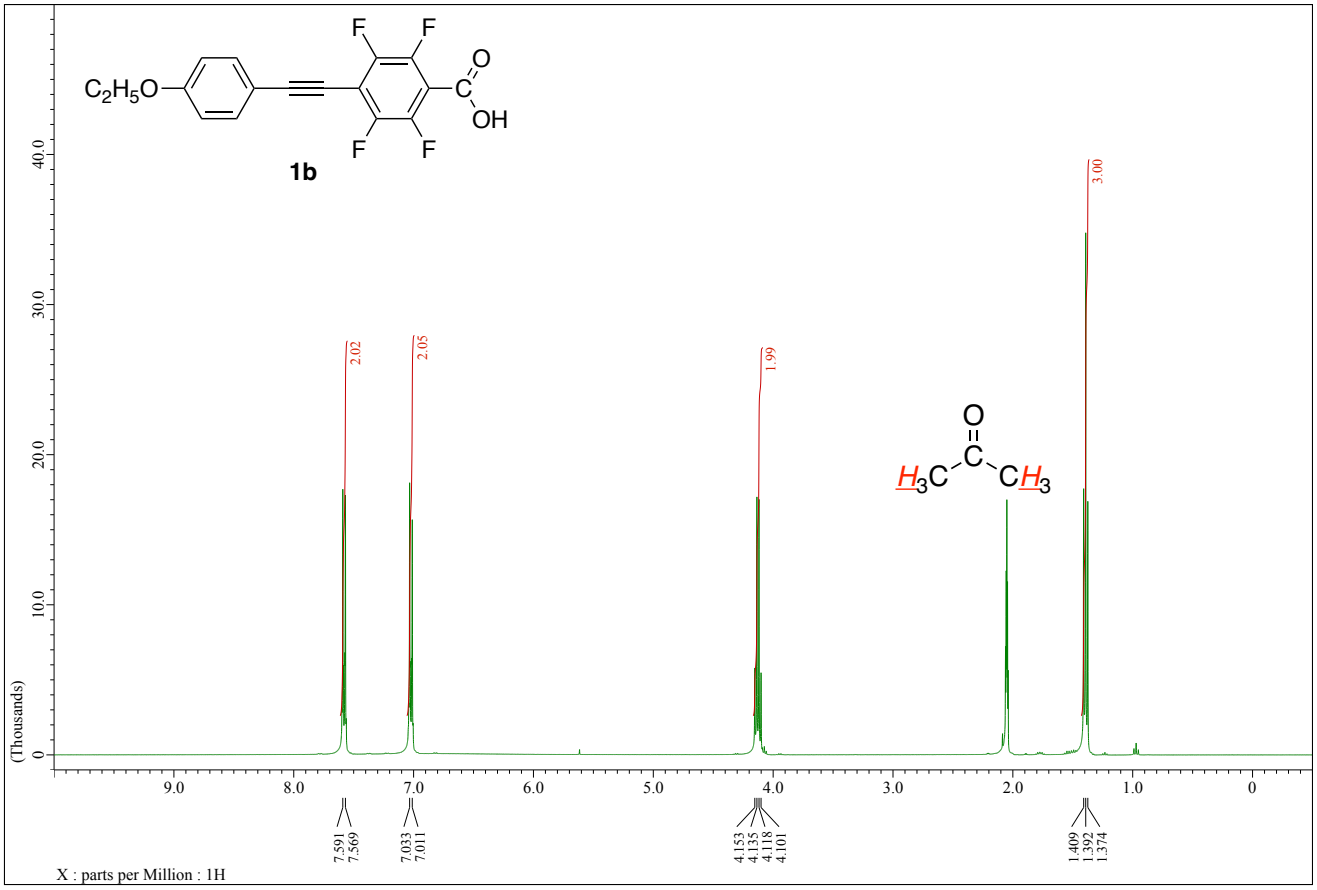

Figure S4. ^{1}H NMR spectrum of **1b** (acetone-d_6, 400 MHz).

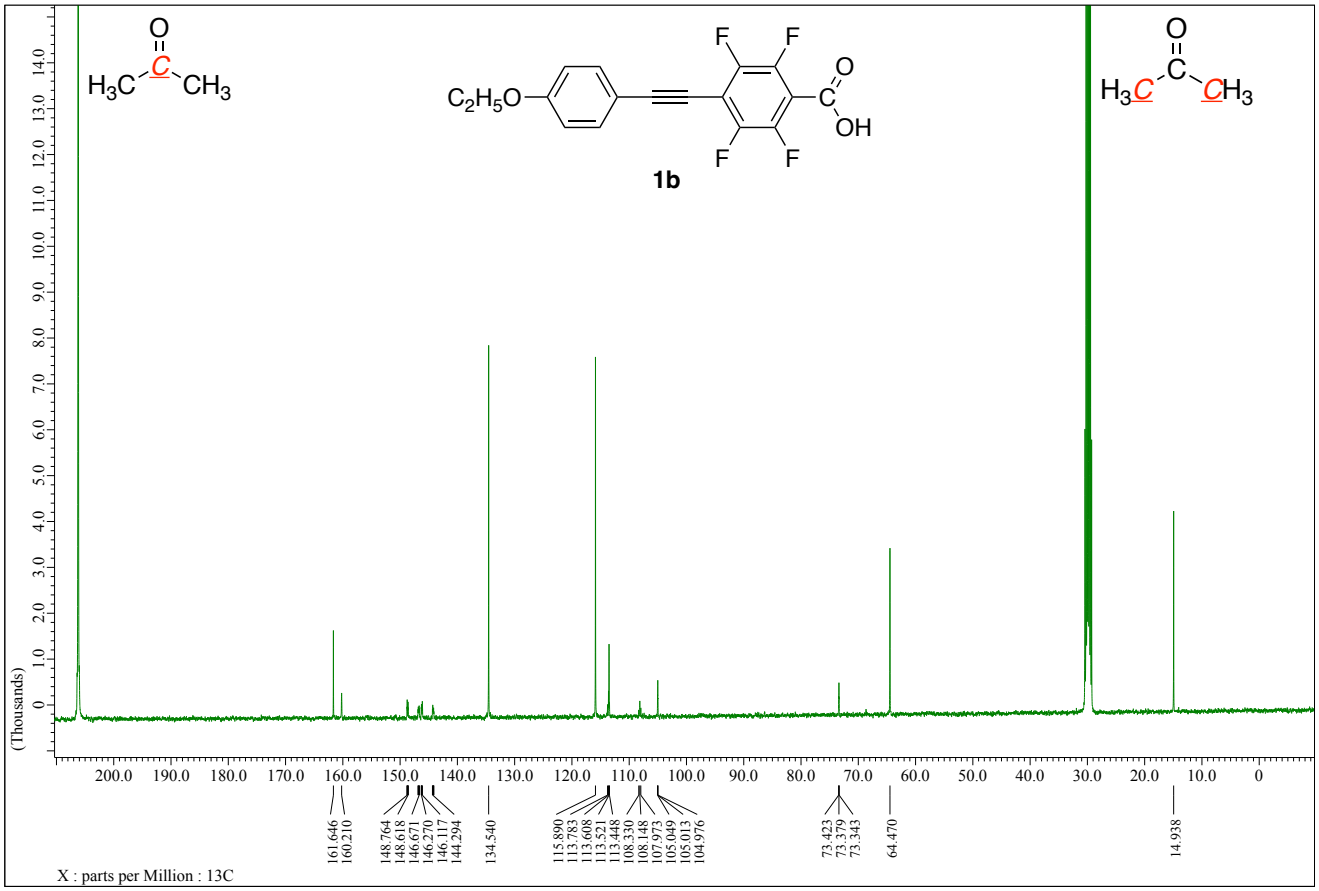

Figure S5. ^{13}C NMR spectrum of **1b** (acetone-d_6, 100 MHz).

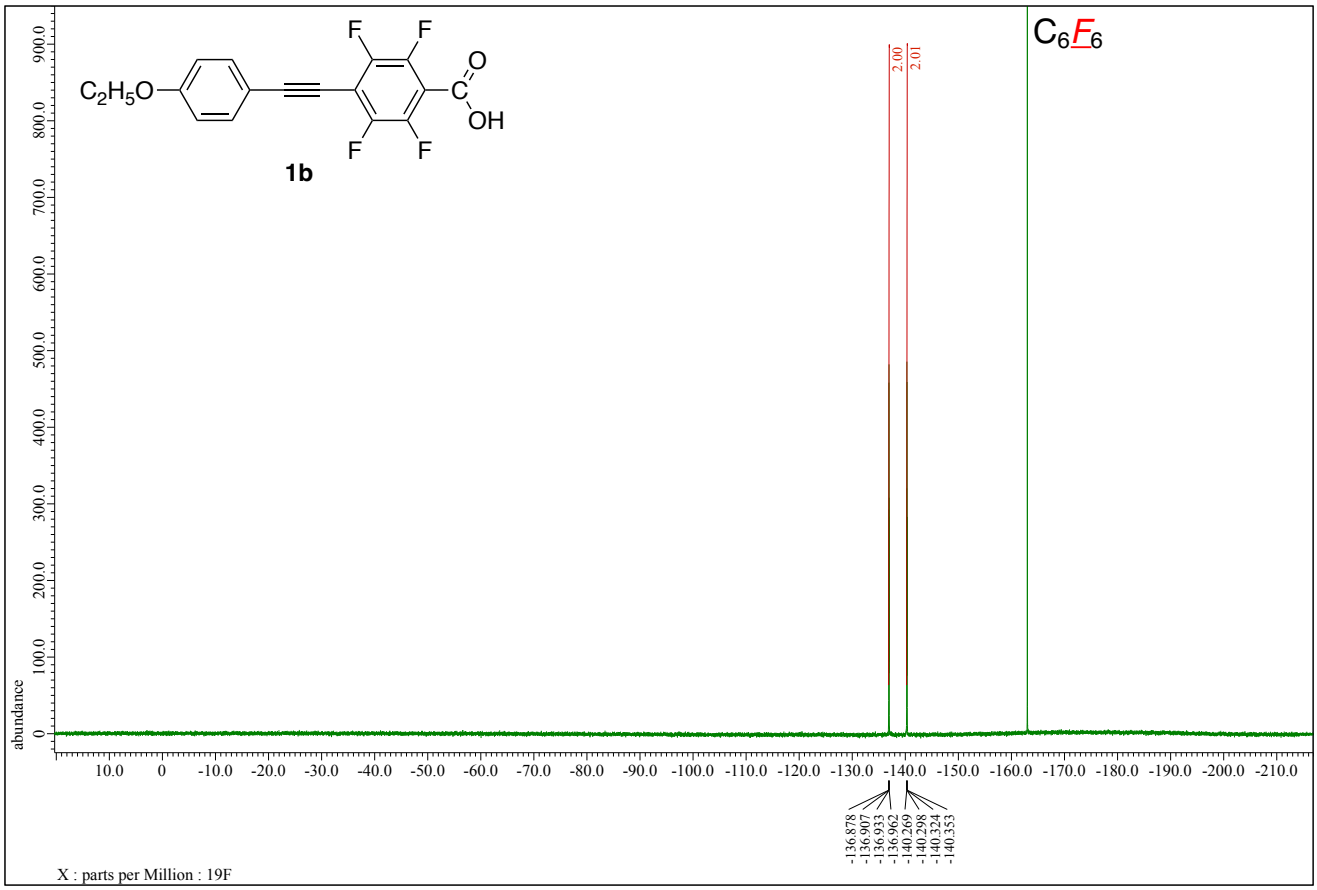

Figure S6. ^{19}F NMR spectrum of **1b** (acetone-d_6, C_6F_6, 376 MHz).

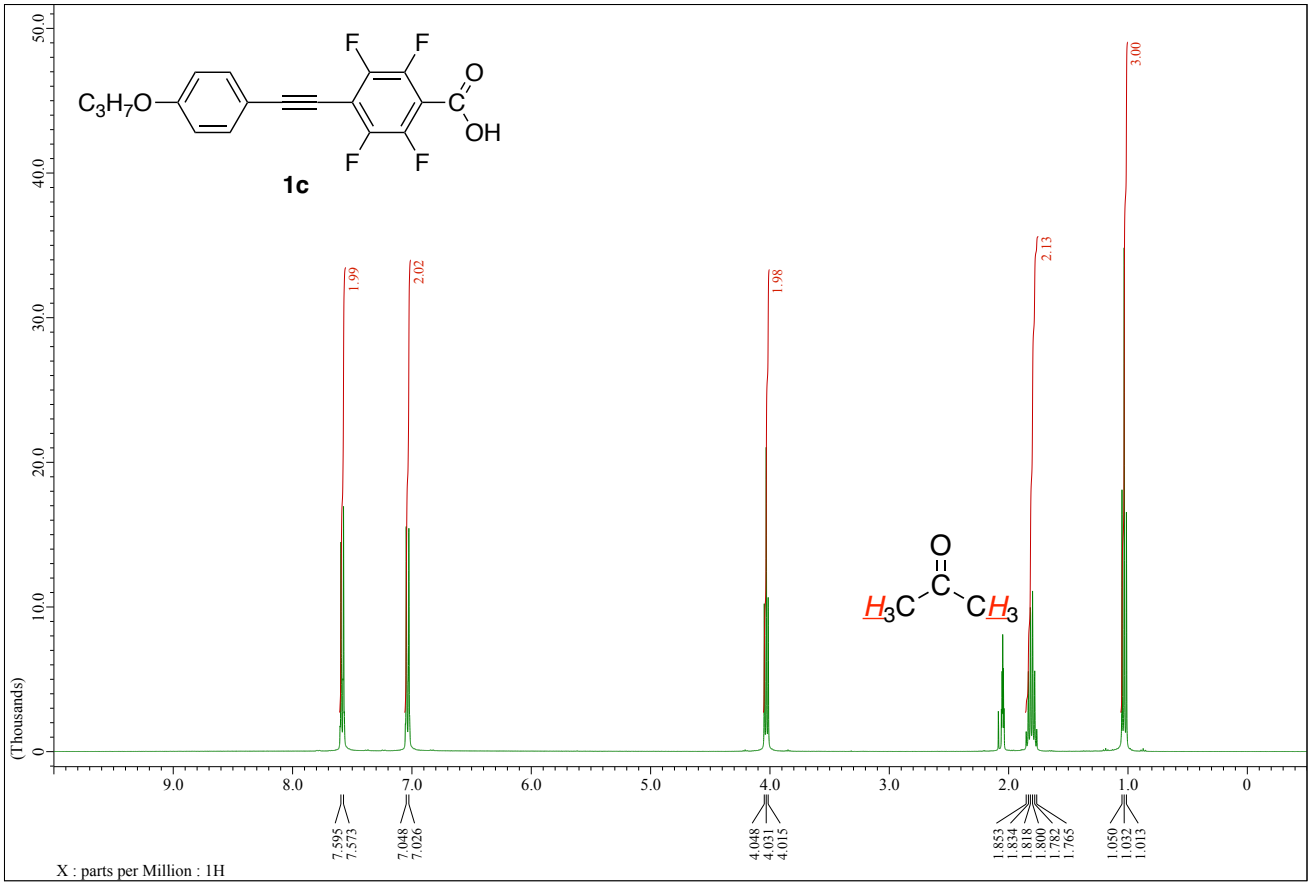

Figure S7. ^{1}H NMR spectrum of **1c** (acetone-d_6, 400 MHz).

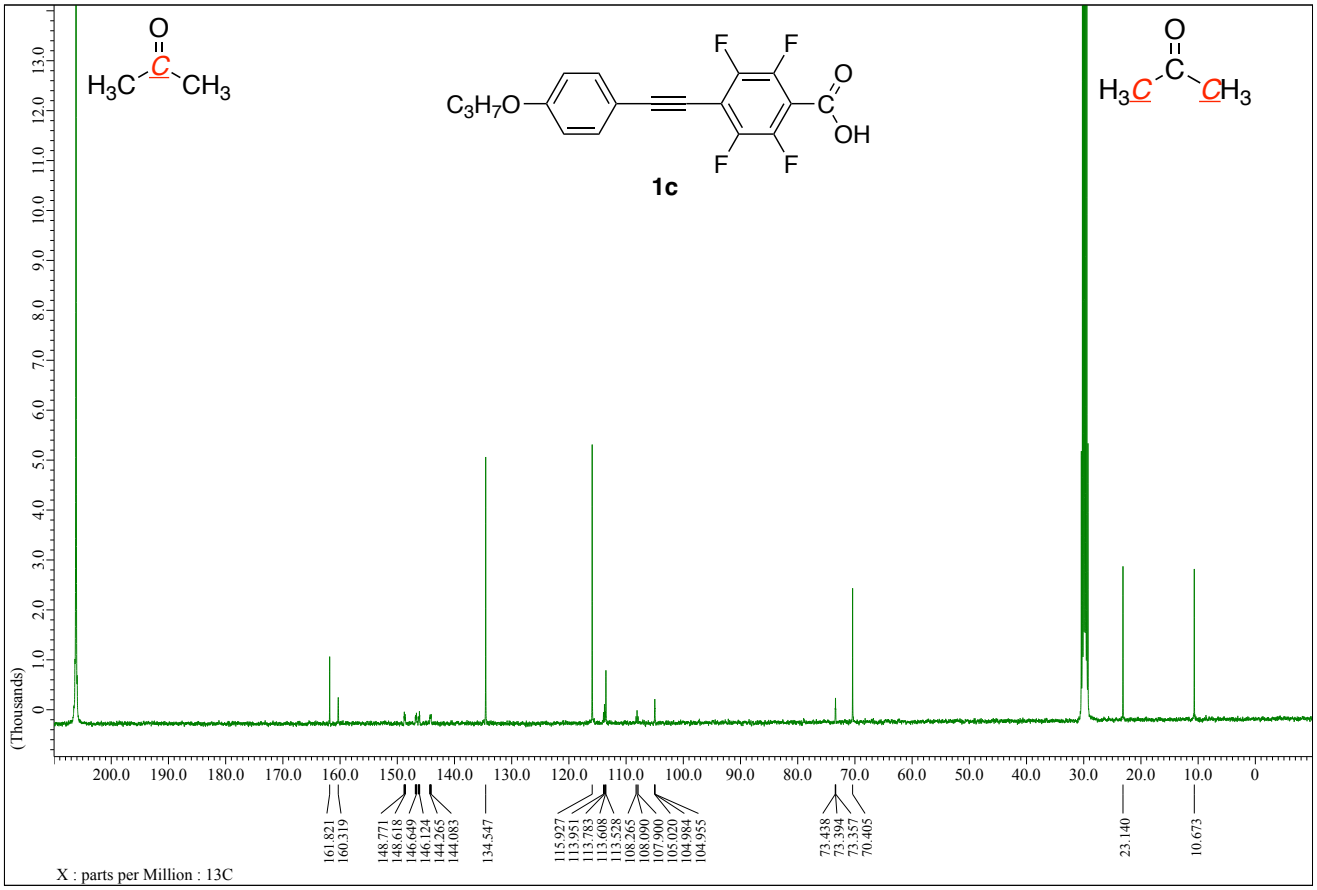

Figure S8. ^{13}C NMR spectrum of **1c** (acetone-d_6, 100 MHz).

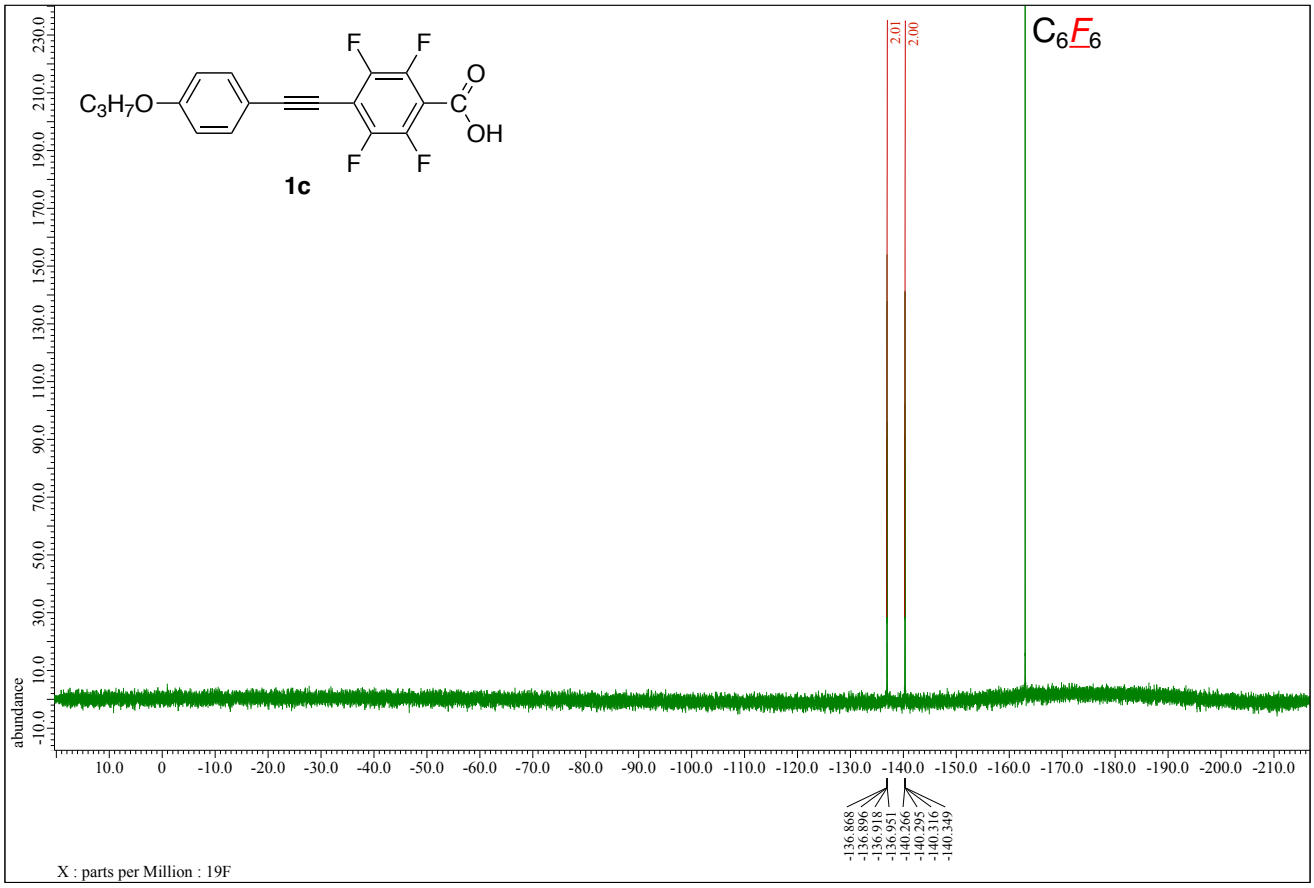

Figure S9. ^{19}F NMR spectrum of **1c** (acetone-d_6, C_6F_6, 376 MHz).

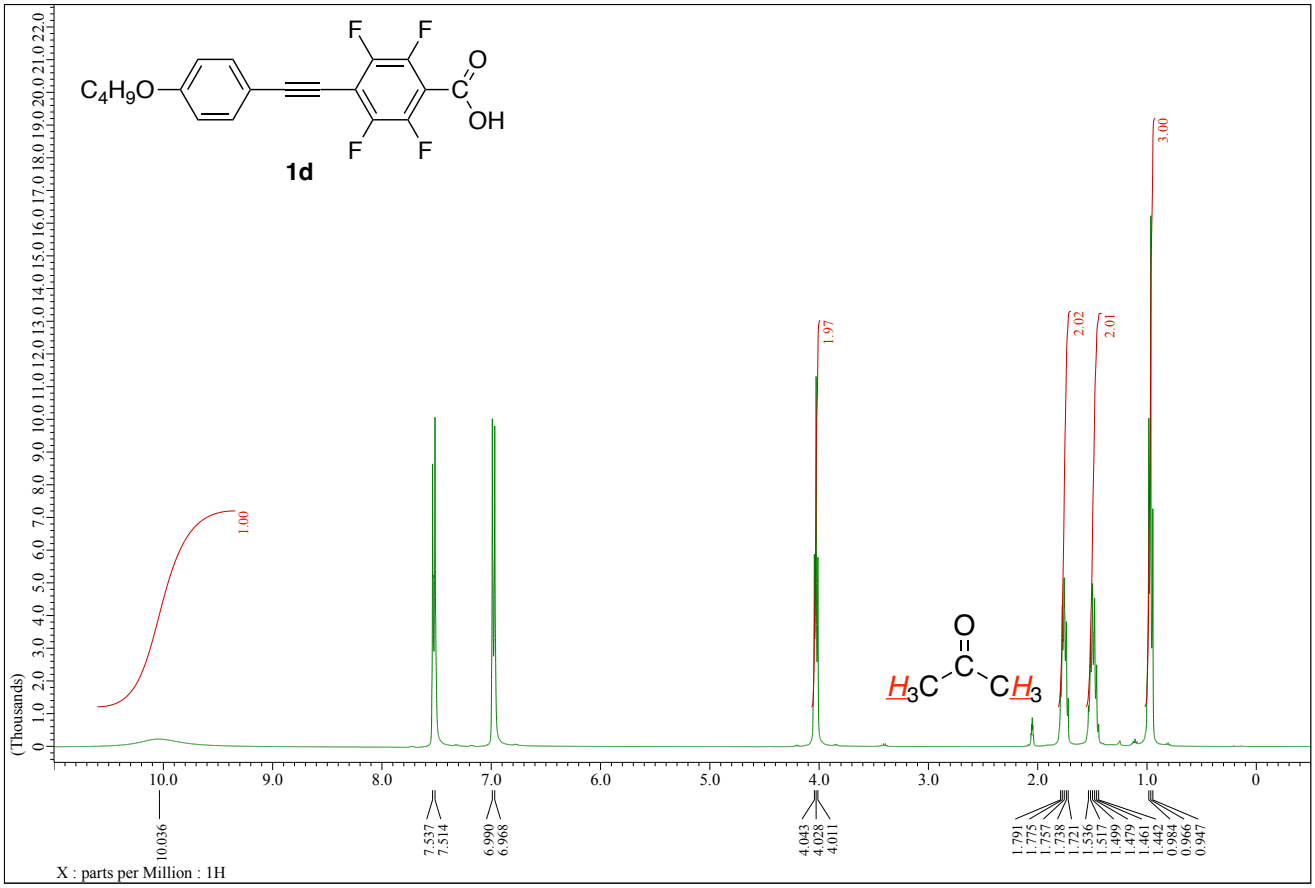

Figure S10. ^{1}H NMR spectrum of **1d** (acetone-d_6, 400 MHz).

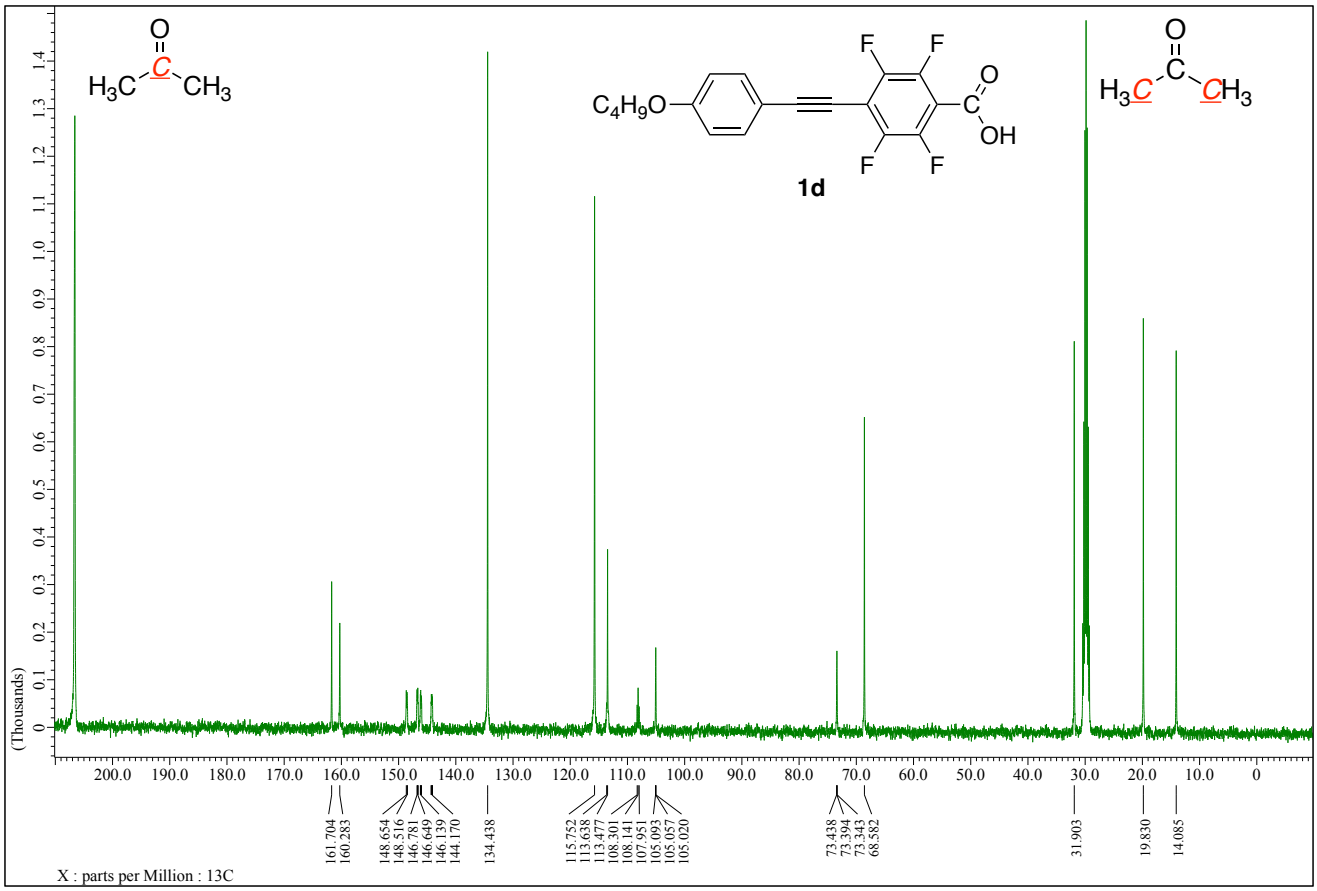

Figure S11. ^{13}C NMR spectrum of **1d** (acetone-d_6, 100 MHz).

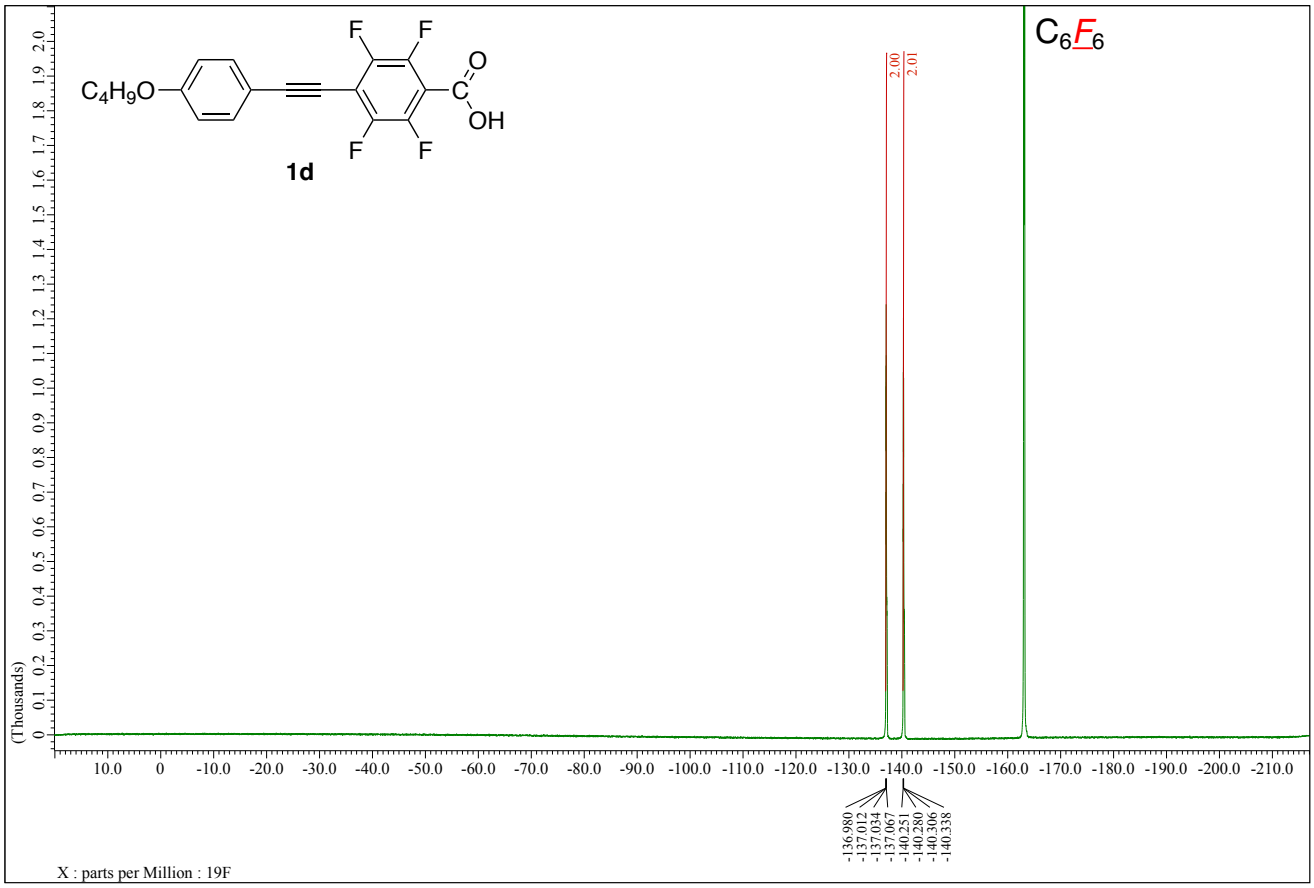

Figure S12. ^{19}F NMR spectrum of **1d** (acetone-d_6, C_6F_6, 376 MHz).

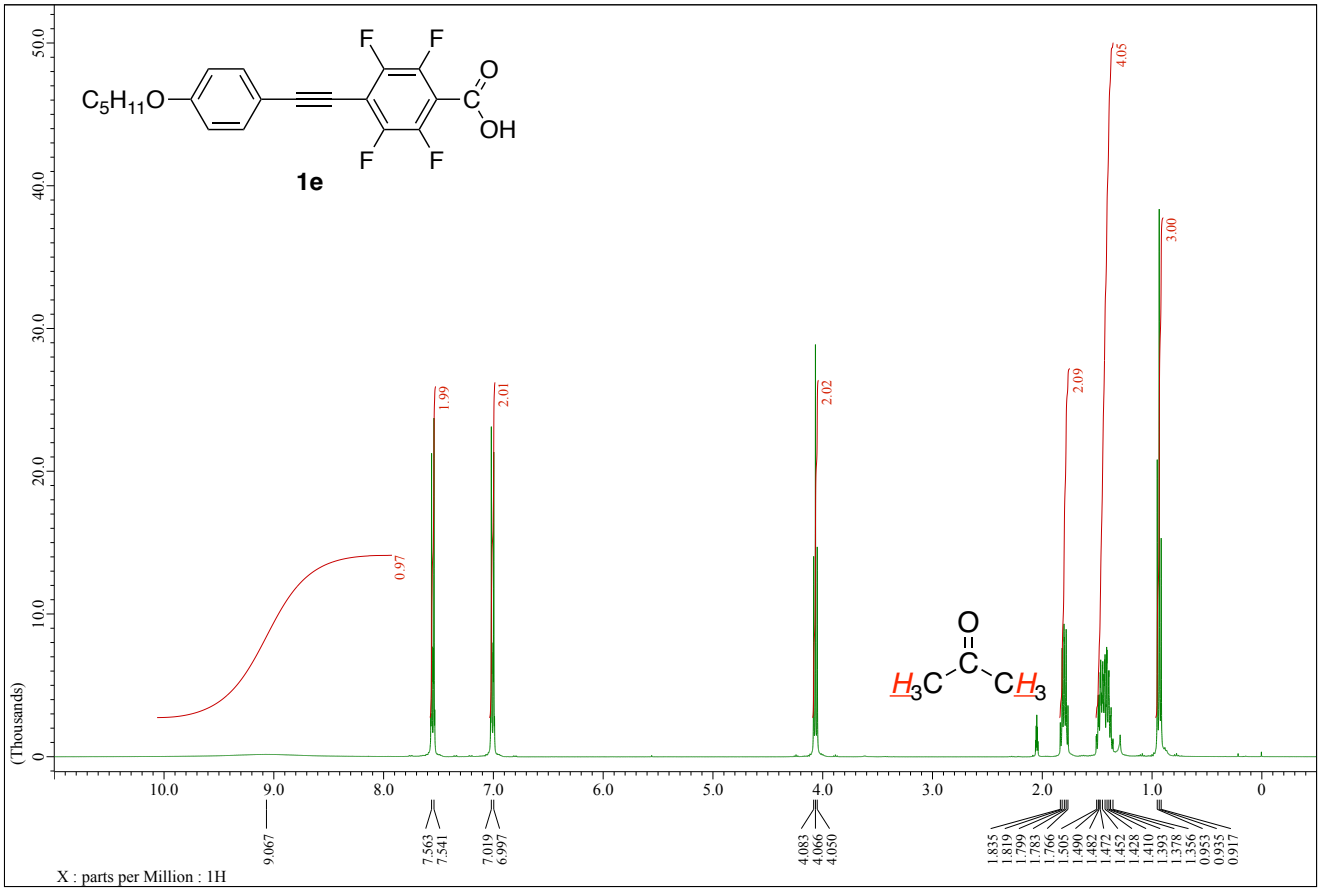

Figure S13. ^{1}H NMR spectrum of **1e** (acetone-d_6, 400 MHz).

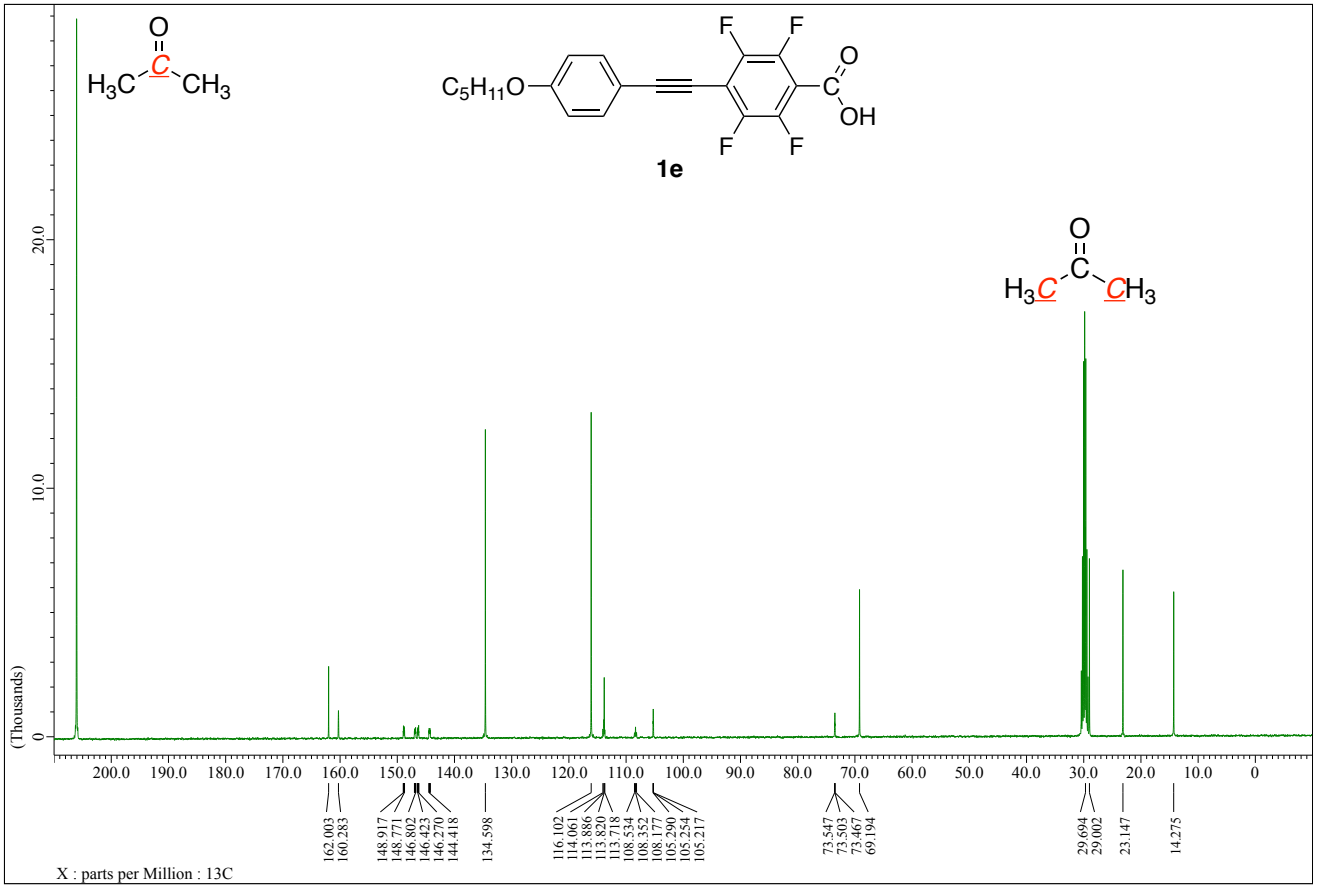

Figure S14. ^{13}C NMR spectrum of **1e** (acetone-d_6, 100 MHz).

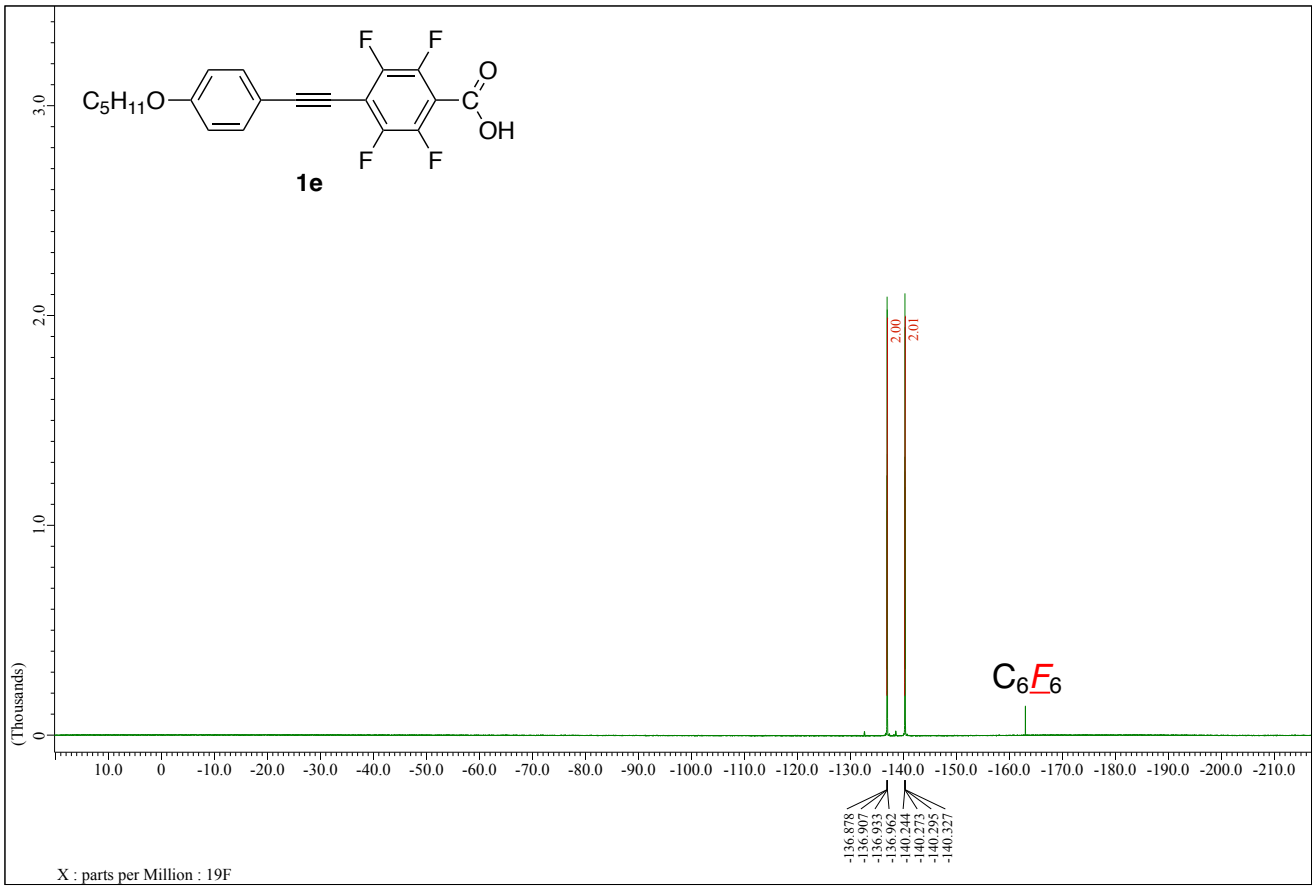

Figure S15. ^{19}F NMR spectrum of **1e** (acetone-d_6, C_6F_6, 376 MHz).

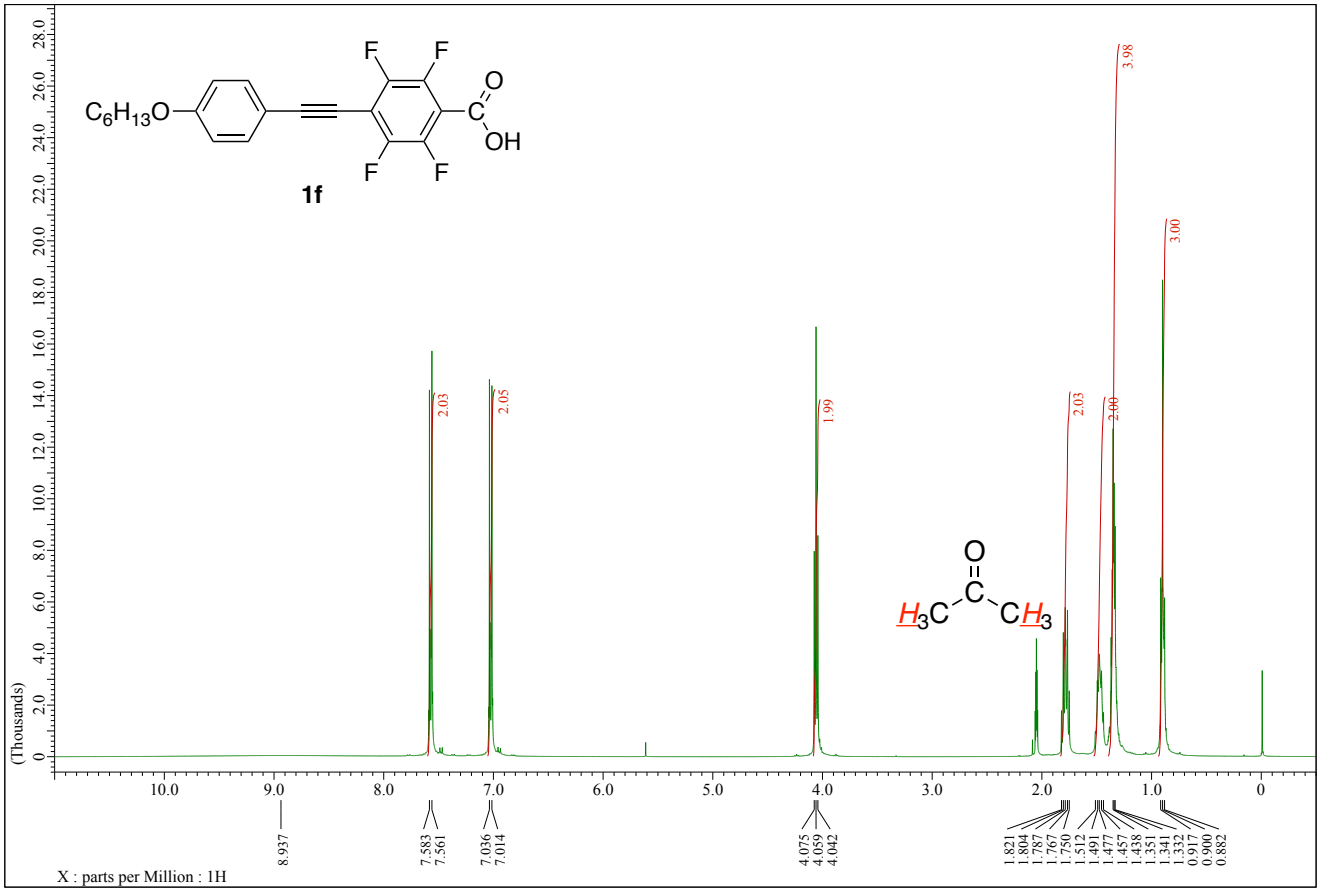

Figure S16. ^{1}H NMR spectrum of **1f** (acetone-d_6, 400 MHz).

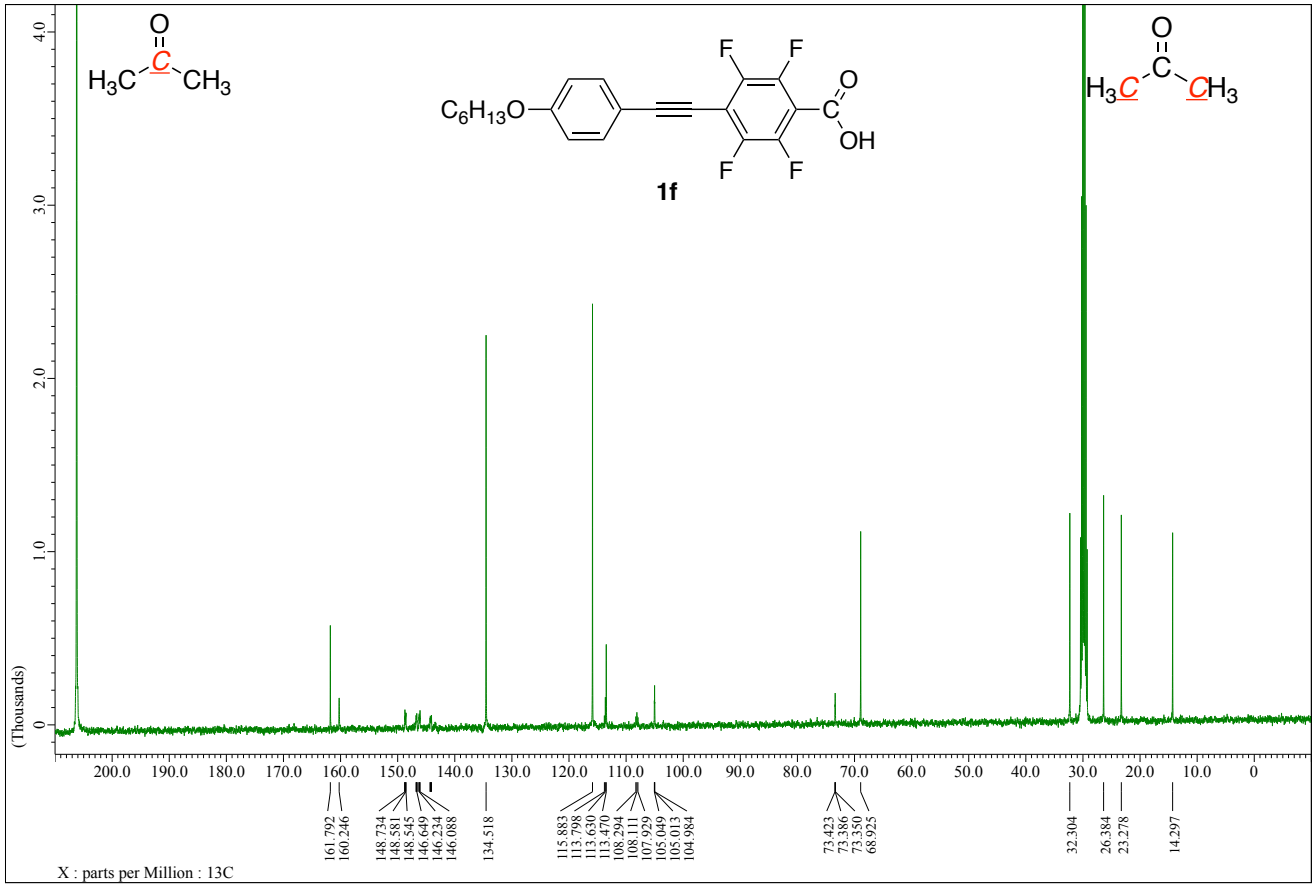

Figure S17. ^{13}C NMR spectrum of **1f** (acetone-d_6, 100 MHz).

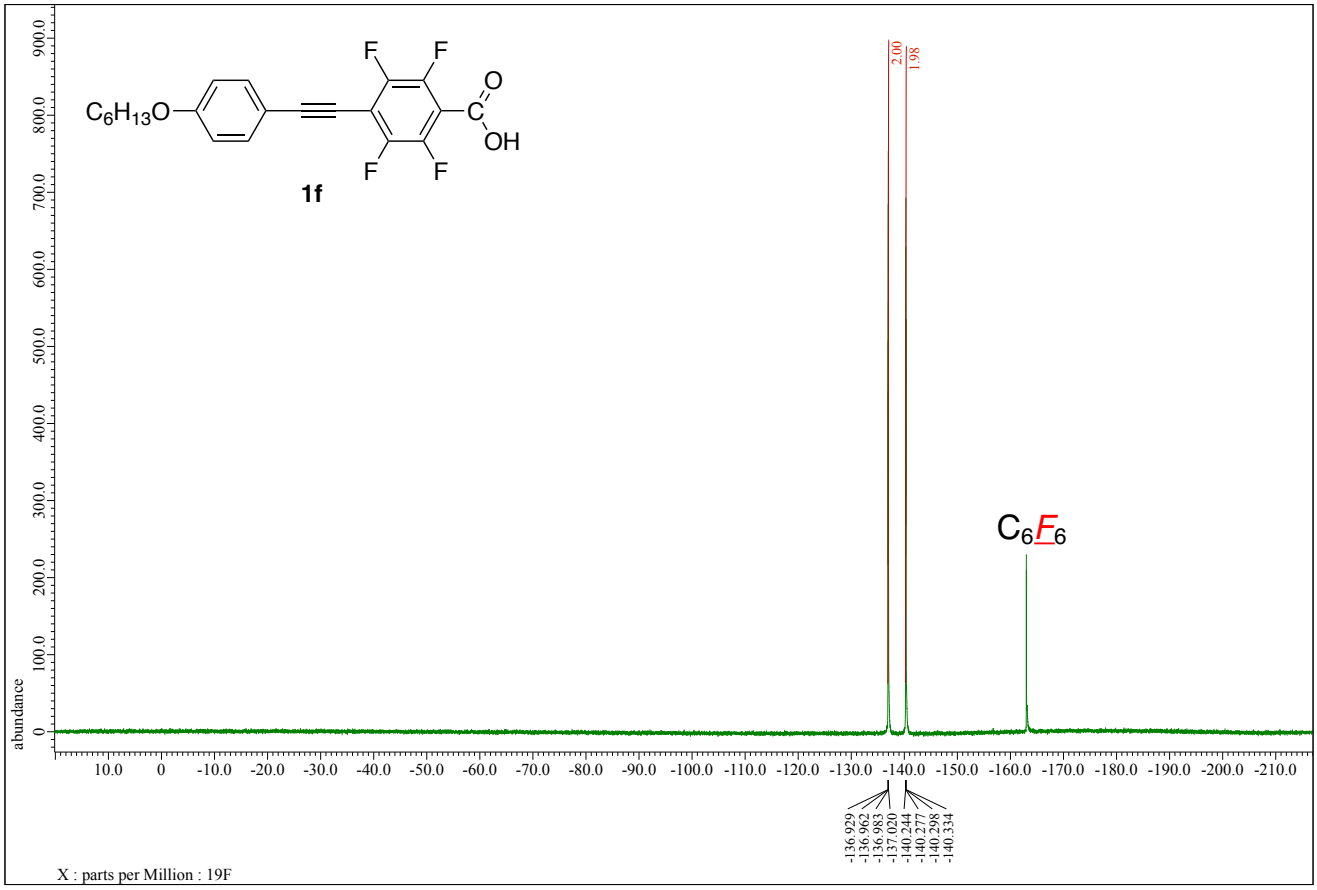

Figure S18. ^{19}F NMR spectrum of **1f** (acetone-d_6, C_6F_6, 376 MHz).

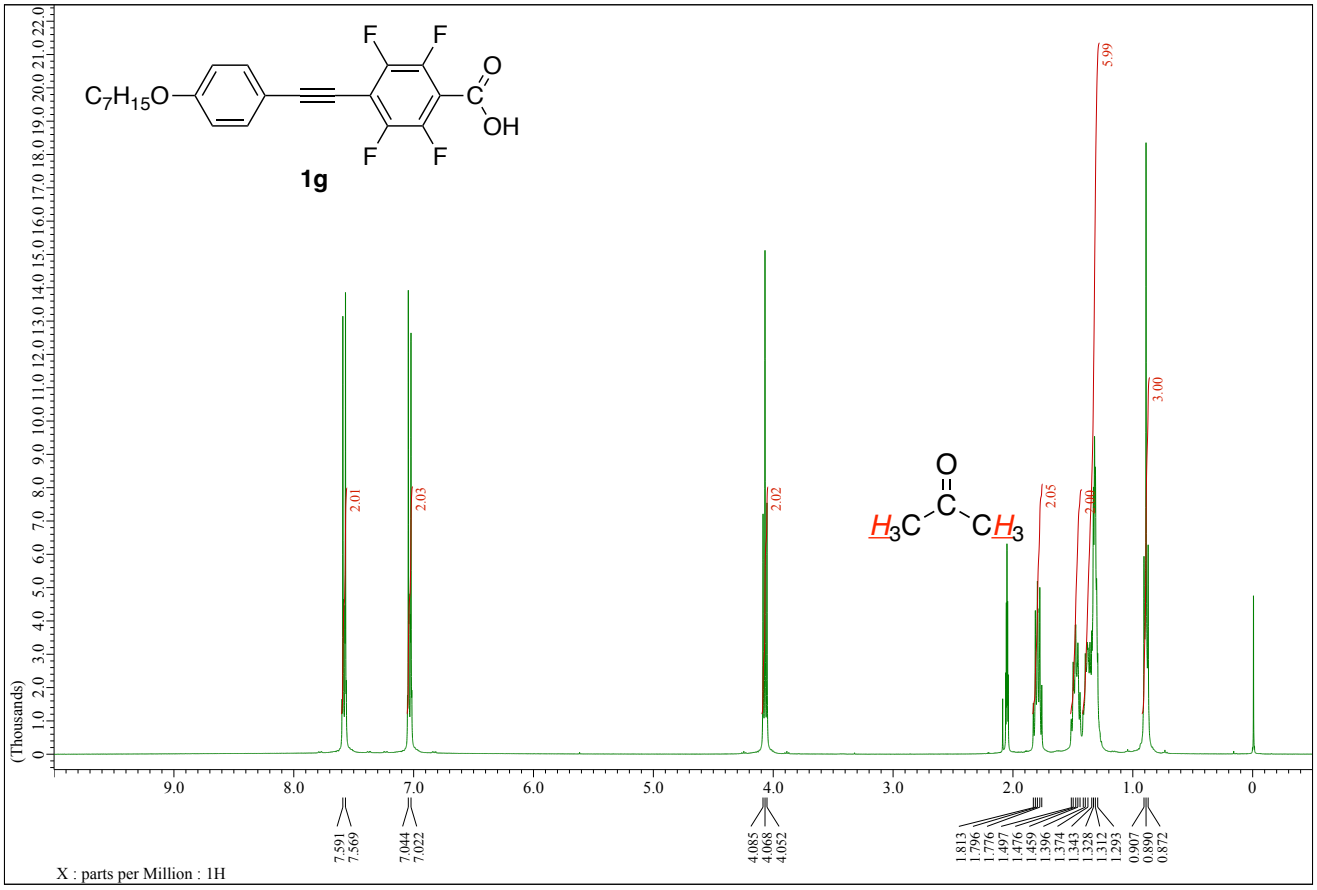

Figure S19. ^{1}H NMR spectrum of **1g** (acetone-d_6, 400 MHz).

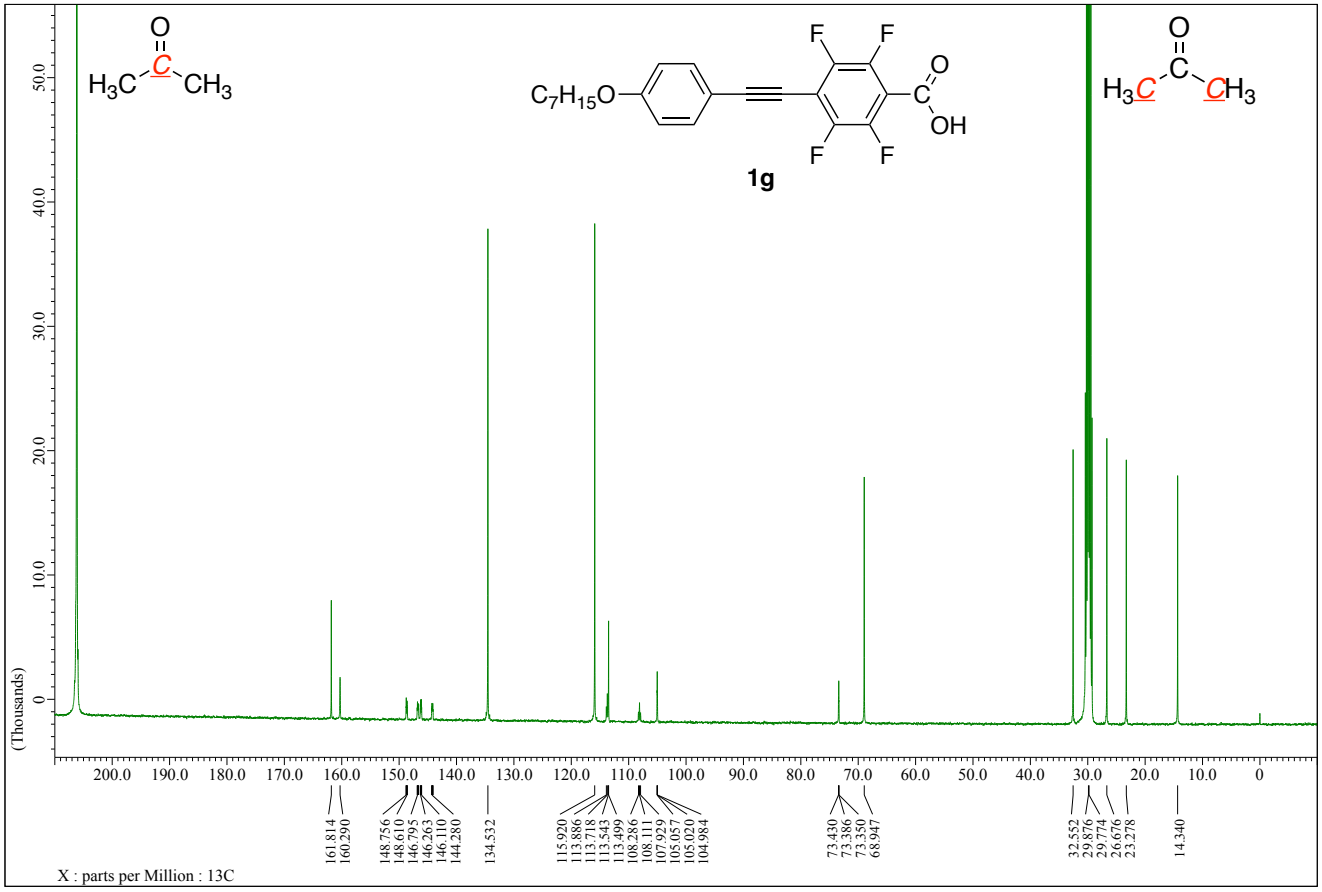

Figure S20. ^{13}C NMR spectrum of **1g** (acetone-d_6, 100 MHz).

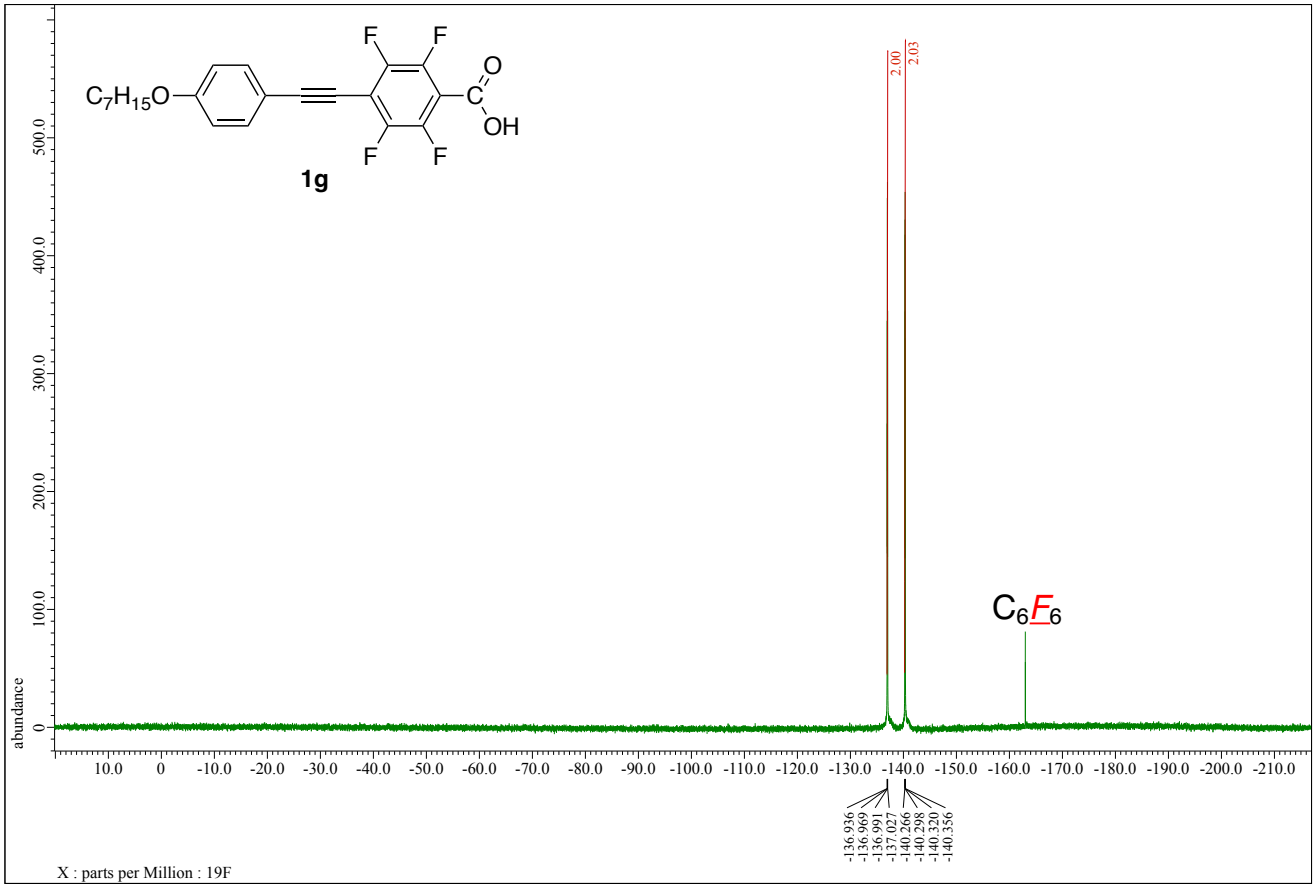

Figure S21. ^{19}F NMR spectrum of **1g** (acetone-d_6, C_6F_6, 376 MHz).

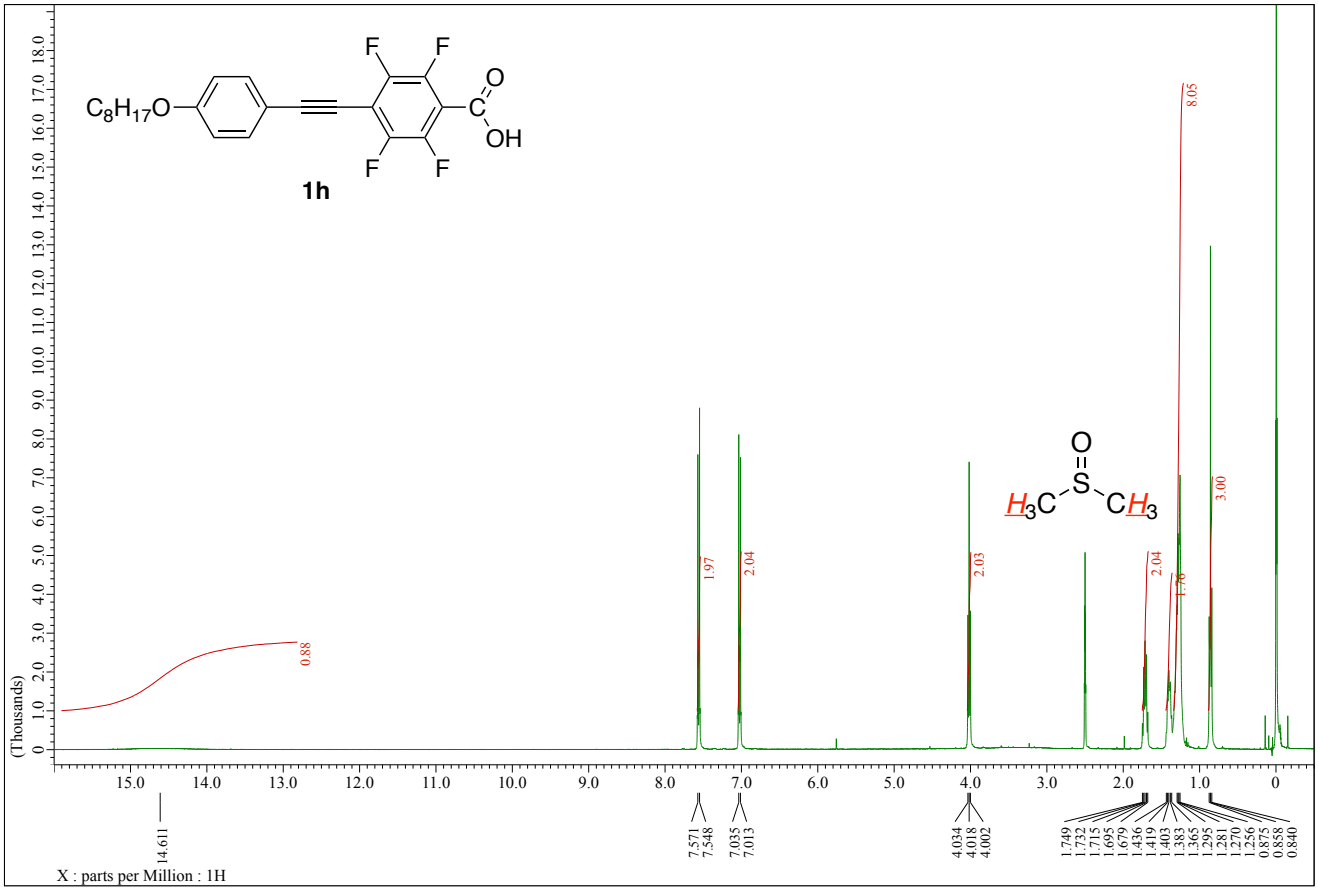

Figure S22. ^{1}H NMR spectrum of **1h** (DMSO-d_6, 400 MHz).

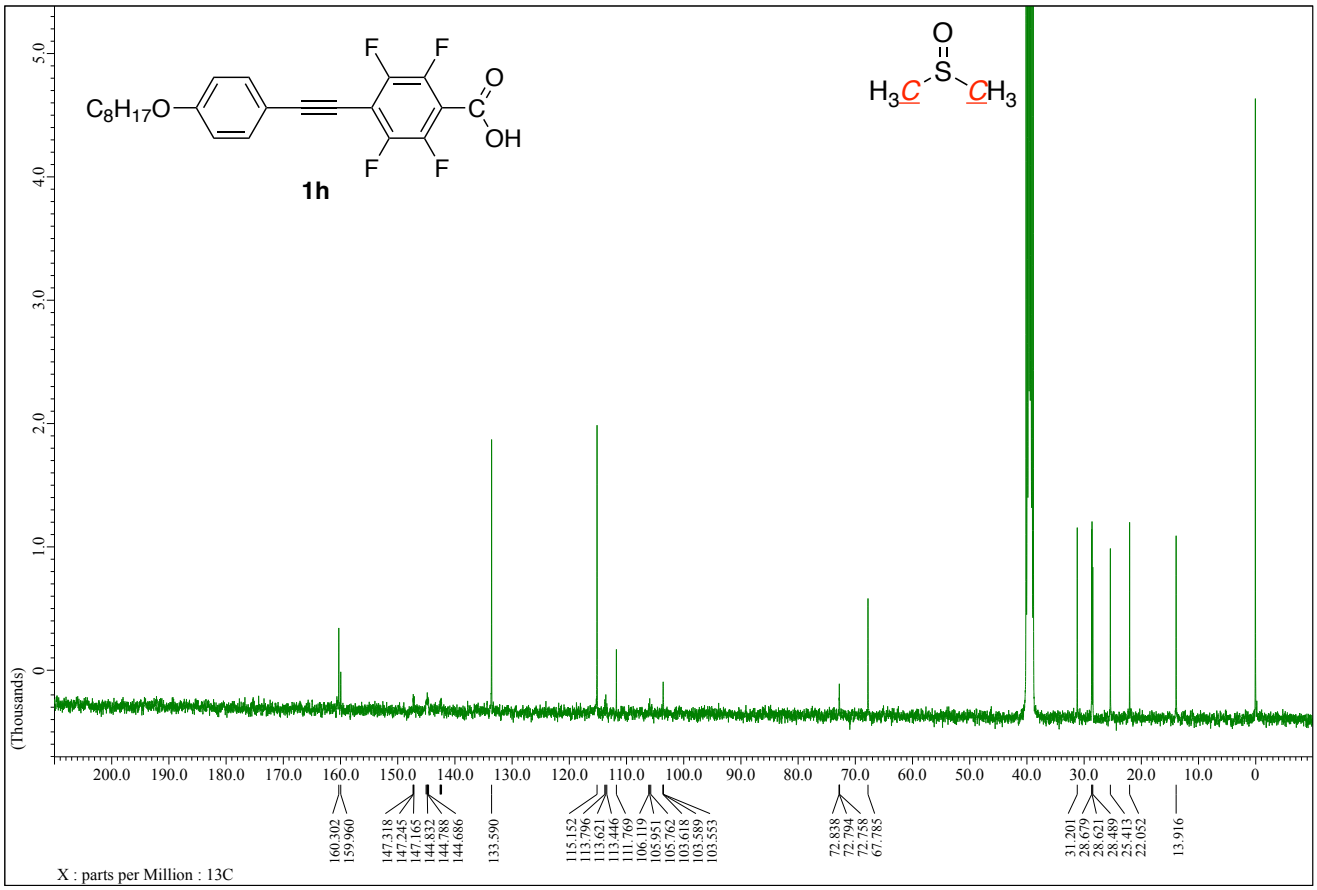

Figure S23. ^{13}C NMR spectrum of **1h** (DMSO-d_6, 100 MHz).

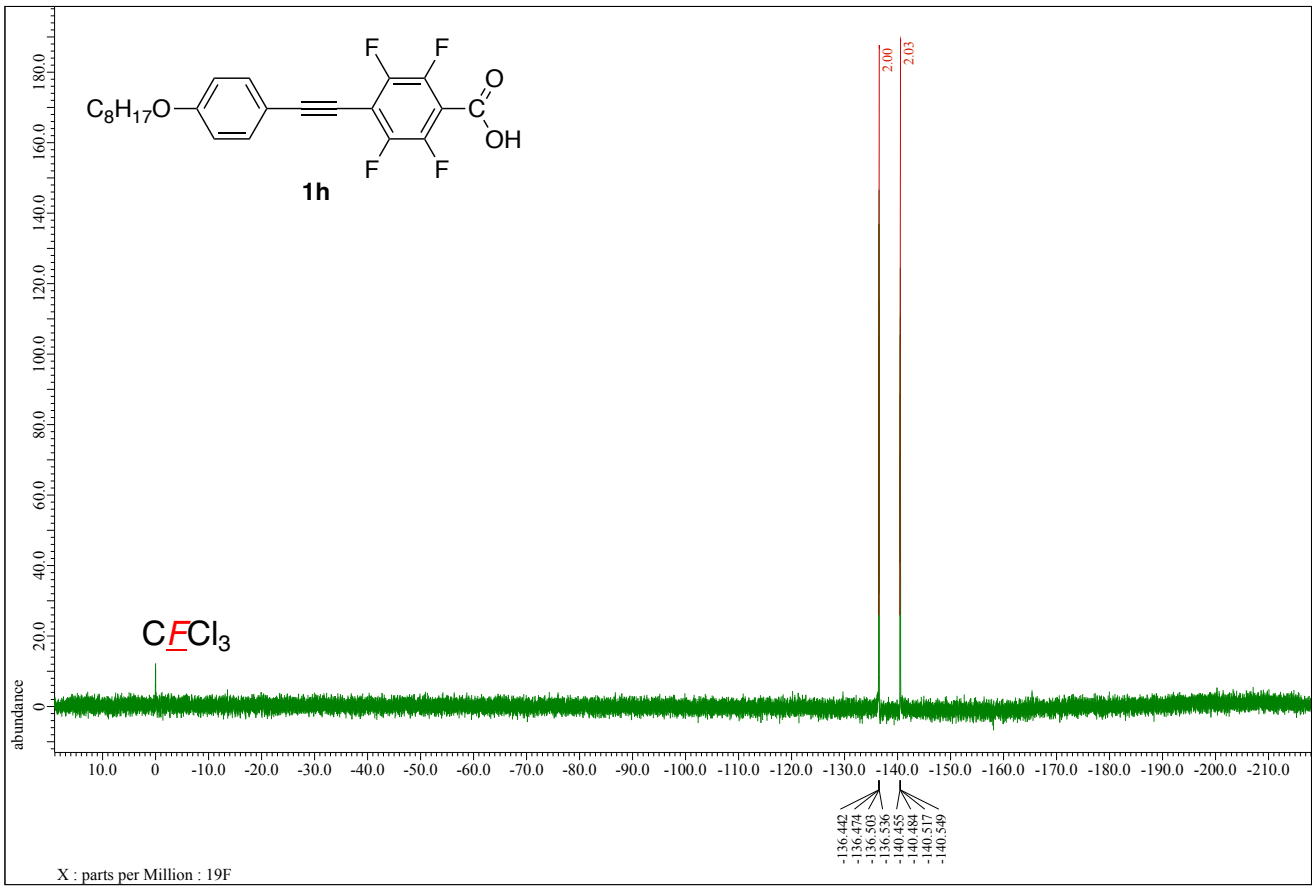

Figure S24. ^{19}F NMR spectrum of **1h** (DMSO-d_6, $CFCl_3$, 376 MHz).

Crystallographic analysis

Single crystal X-ray diffractions were recorded on an XtaLab AFC11 diffractometer (Rigaku). The reflection data were integrated, scaled, and averaged using CrysAlisPro (ver. 1.171.39.43a, Rigaku). Empirical absorption corrections were applied using the SCALE 3 ABSPACK scaling algorithm (CrysAlisPro). The structure were identified by a direct method (SHELXT-2018/2) and refined using a full matrix least square method (SHELXL-2014/7) visualized by Olex2. The crystallographic data were deposited into the Cambridge Crystallographic Data Centre (CCDC) database. These data can be obtained free of charge from the CCDC via www.ccdc.cam.ac.uk/data_request/cif.

Table S1. Crystallographic data of **1a** and **1e**

	1a	**1e**
CCDC #	2193549	2193550
Empirical Formula	$C_{16}H_8F_4O_3$	$C_{20}H_{16}F_4O_3$
Formula weight	324.22	380.33
Temperature [K]	293	293
Crystal Color / Habit	Colourless / Block	Colourless / Block
Crystal Size [mm]	0.542 x 0.293 x 0.231	0.550 x 0.330 x 0.190
Crystal System	Triclinic	Monoclinic
Space Group	$P\,\bar{1}$	$C2/c$
a [Å]	6.4440(3)	23.399(4)
b [Å]	7.329(3)	8.7158(7)
c [Å]	15.3823(7)	19.649(2)
α [°]	95.185(3)	90
β [°]	100.896(4)	115.880(14)
γ [°]	99.639(3)	90
V [Å^3]	701.88(6)	3605.3(8)
Z	2	8
R [$F^2 > 2s(F^2)$] [a]	0.0480	0.0559
wR_2 (F^2) [b]	0.1528	0.1888

[a] $R = \Sigma||F_o| - |F_c|| \,/\, \Sigma|F_o|$. [b] $wR = \{[\Sigma w(|F_o| - |F_c|)]/\Sigma w|F_o|\}^{1/2}$.

Phase transition behavior

(a) **1a**

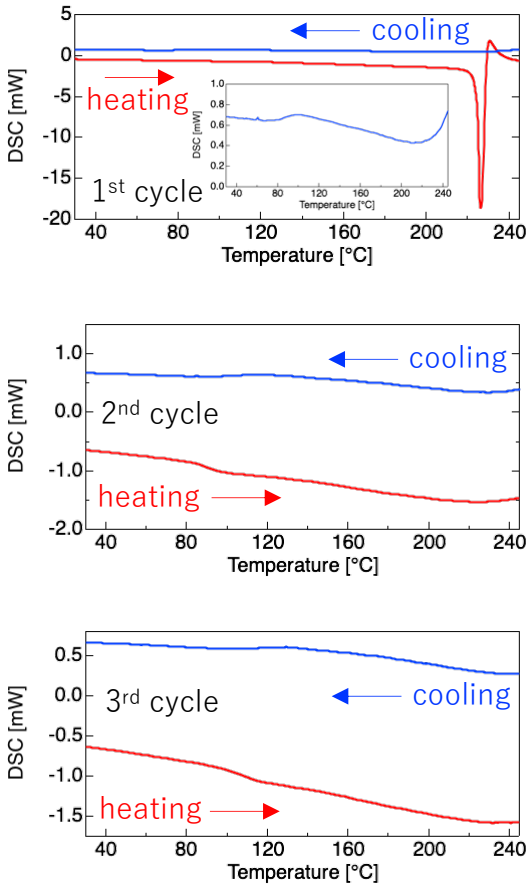

(b) **1b**

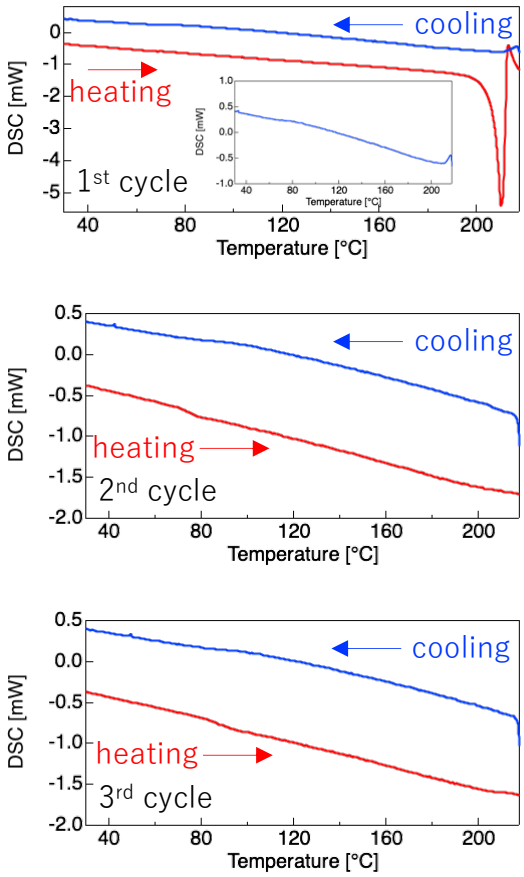

(c) **1c**

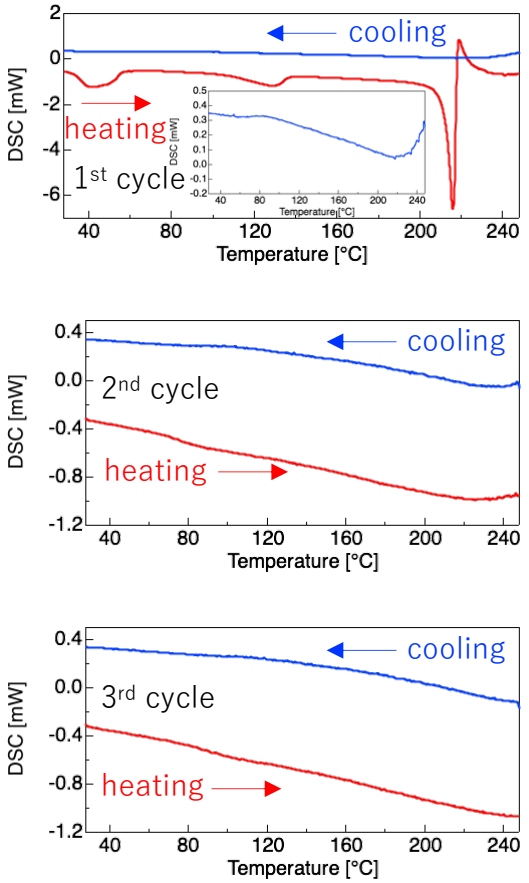

(d) **1d**

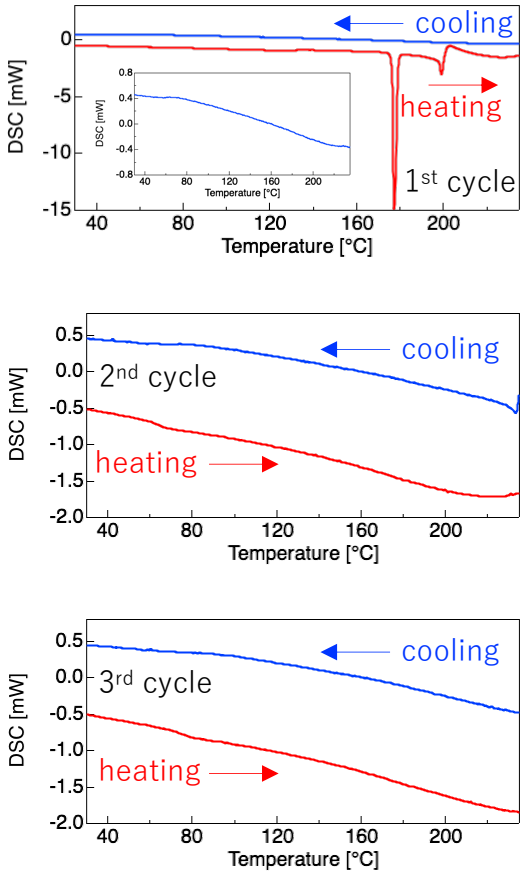

(e) **1e**

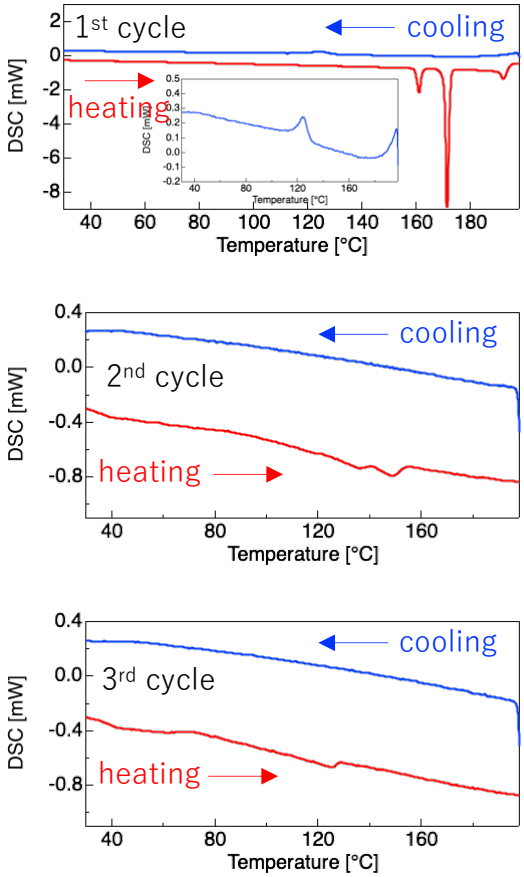

(f) **1f**

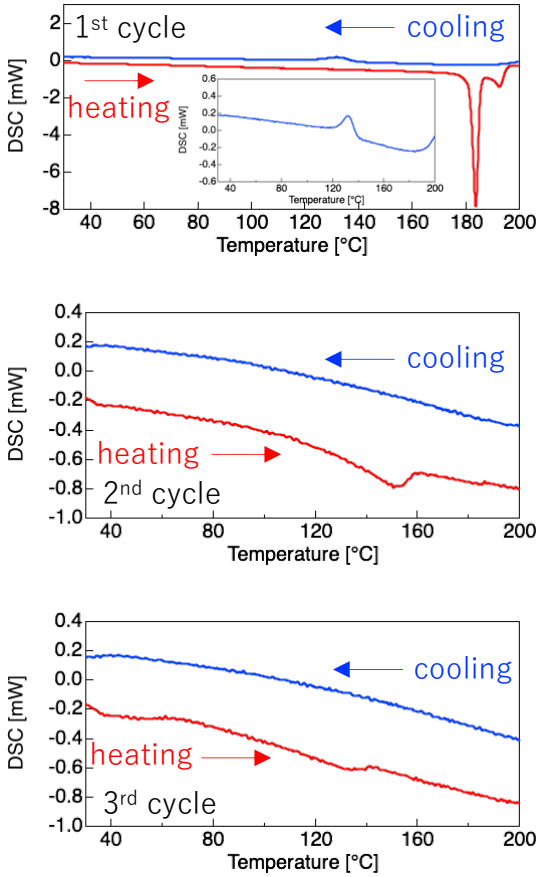

(g) **1g**

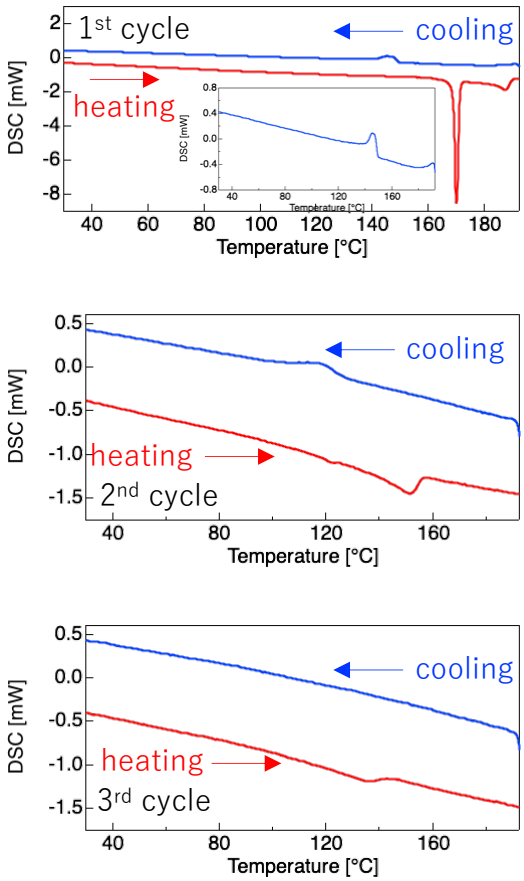

(h) **1h**

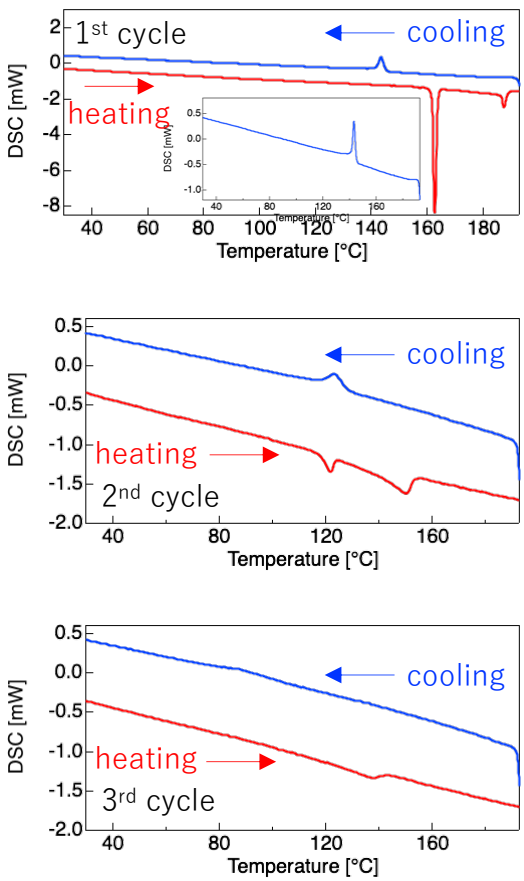

Figure S25. DSC Thermograms of **1a**–**h** under N_2 atmosphere. Scan rate: 5.0 °C min^{-1} or 10 °C min^{-1}.

Table S2. Phase transition behavior of **1a**–**h** observed by DSC measurement.

Molecule	Phase sequence		Temperature [°C]	Enthalpy (ΔH) [kJ mol^{-1}]	Entropy (ΔS) [J mol^{-1} K^{-1}]
1a	1st Heating	Cry-Iso	224	47.4	96.0
	1st Cooling	Iso-G	165	– [a]	– [a]
	2nd Heating	G-Iso	158	– [a]	– [a]
	2nd Cooling	Iso-G	168	– [a]	– [a]
1b	1st Heating	Cry-Iso	207	44.8	91.0
	1st Cooling	Iso-G	140	–	–
	2nd Heating	G-Iso	137	– [a]	– [a]
	2nd Cooling	Iso-G	146	– [a]	– [a]
1c	1st Heating	Cry-Iso	211	49.6	102.0
	1st Cooling	Iso–Cry	158	– [a]	– [a]
	2nd Heating	G-Iso	142	– [a]	– [a]
	2nd Cooling	Iso-G	137	– [a]	– [a]
1d	1st Heating	Cry-N	176	29.9	66.7
		N-Iso	198	7.27	15.4
	1st Cooling	Iso-G	124	– [a]	– [a]
	2nd Heating	G-Iso	111	– [a]	– [a]
	2nd Cooling	Iso-G	105	– [a]	– [a]
1e	1st Heating	Cry^1-Cry^2	160	8.9	20.4
		Cry^2-N	170	39.3	88.6
		N-Iso	191	5.0	10.8
	1st Cooling	Iso-G	132	– [a]	– [a]
	2nd Heating	G-Iso	137	– [a]	– [a]
	2nd Cooling	Iso-G	134	– [a]	– [a]
1f	1st Heating	Cry-N	181	27.2	60.0
		N-Iso	190	3.77	8.14
	1st Cooling	Iso-G	141	– [a]	– [a]
	2nd Heating	G-Iso	122	– [a]	– [a]
	2nd Cooling	Iso-G	121	– [a]	– [a]
1g	1st Heating	Cry-N	169	29.2	66.1
		N-Iso	184	7.63	16.7
	1st Cooling	Iso-G	150	−5.03	−11.9
	2nd Heating	G-Iso	131	– [a]	– [a]
	2nd Cooling	Iso-G	127	– [a]	– [a]
1h	1st Heating	Cry-N	161	31.2	71.6
		N-Iso	186	5.53	12.0
	1st Cooling	Iso-N	146	−7.01	−16.8
	2nd Heating	G-N	118	– [a]	– [a]

	N-Iso	137	– [a]	– [a]
2nd Cooling	Iso-G	131	– [a]	– [a]

[a] Determined by POM observation.

TG Analysis

(a) **1a**

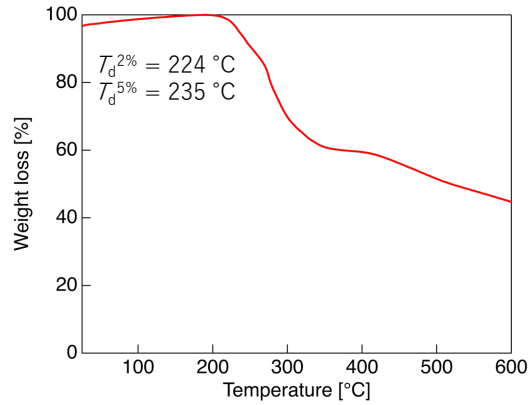

(b) **1b**

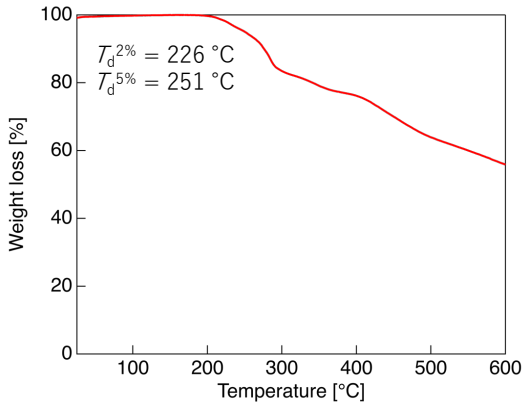

(c) **1c**

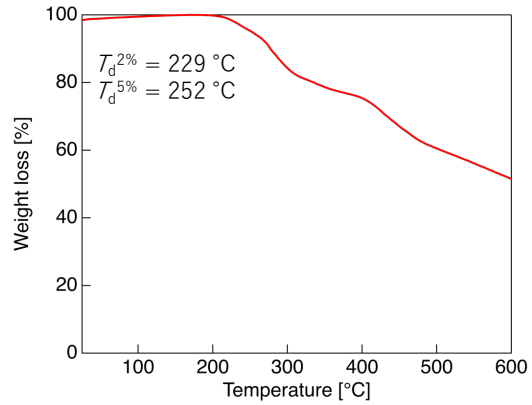

(d) **1d**

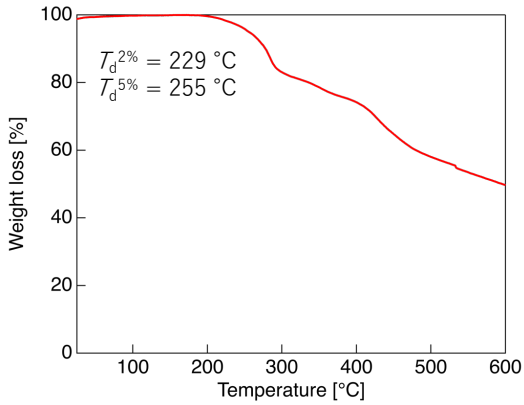

(e) **1e**

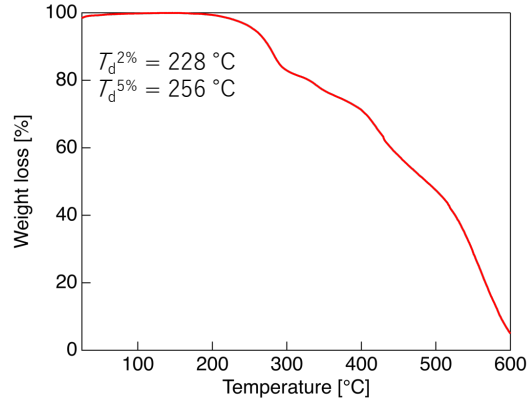

(f) **1f**

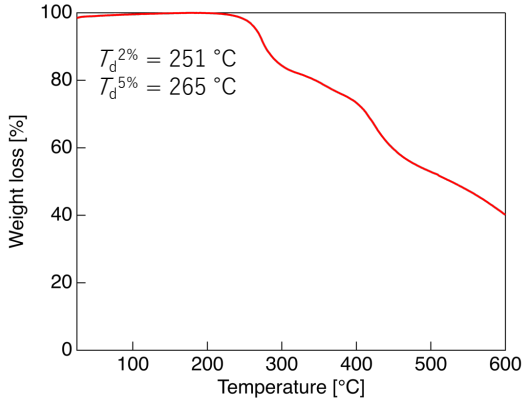

(g) **1g**

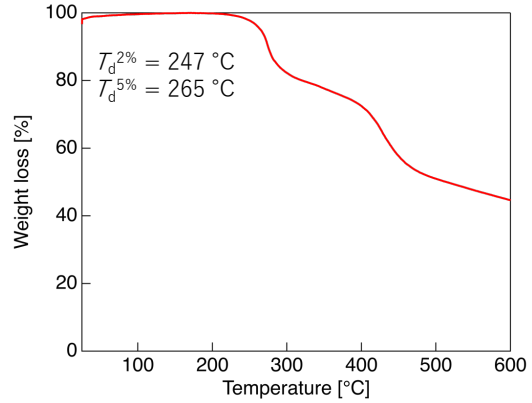

(h) **1h**

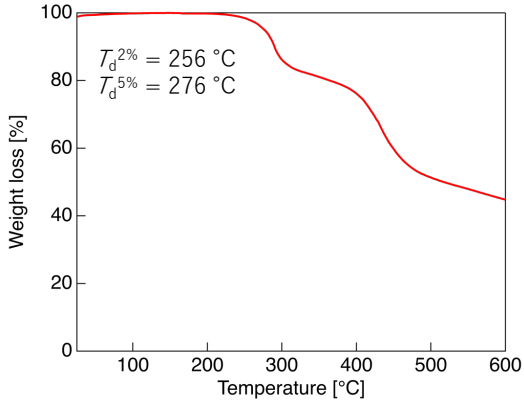

Figure S26. TGA Thermograms of **1a**–**h** under N_2 atmosphere. Scan rate: 10 °C min^{-1}.

(a) **1d**

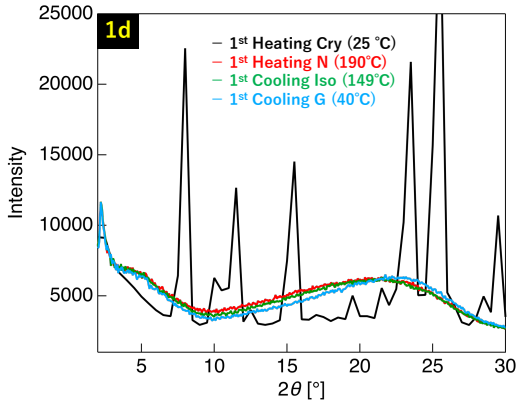

(b) **1e**

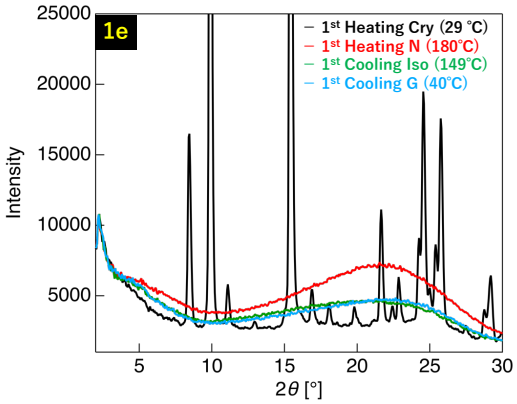

(c) **1f**

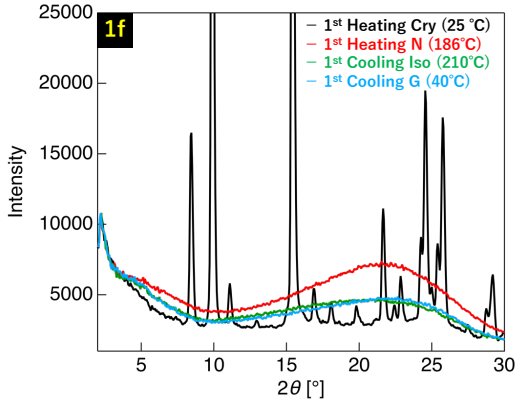

(d) **1g**

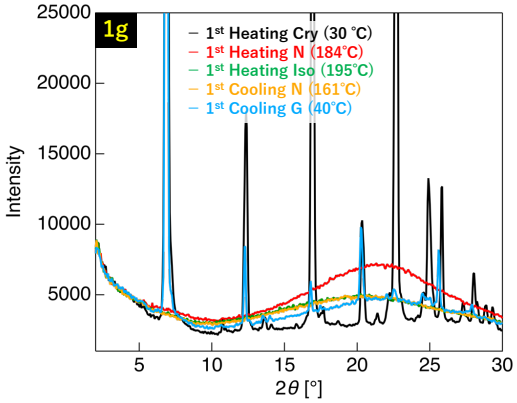

(e) **1h**

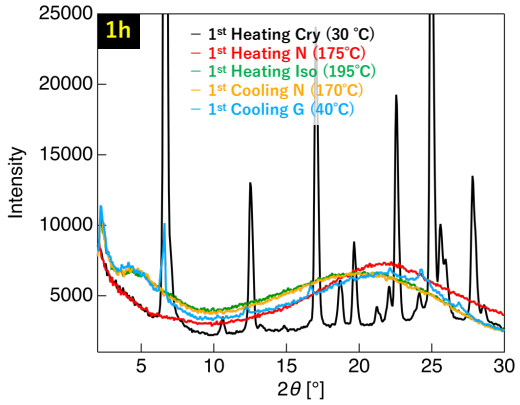

Figure S27. VT-PXRD pattern of **1d**–**h** during the 1st heating and cooling processes.

Photophysical behavior

CH_2Cl_2 solution phase

(a) **1a**

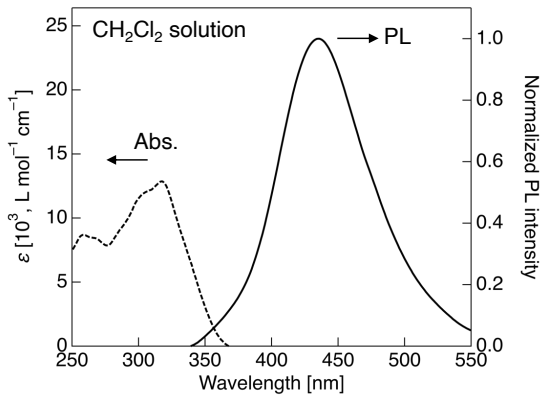

(b) **1b**

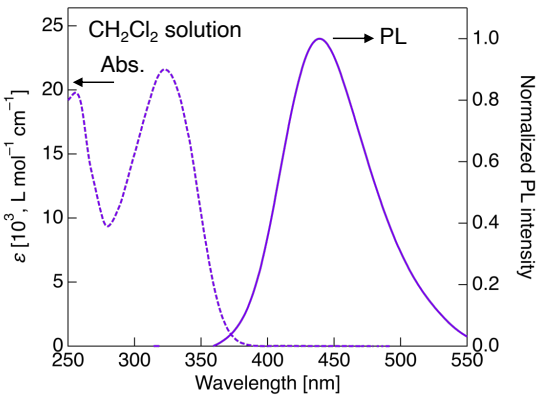

(c) **1c**

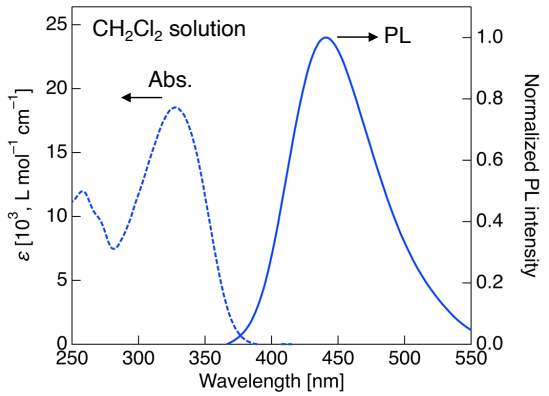

(d) **1d**

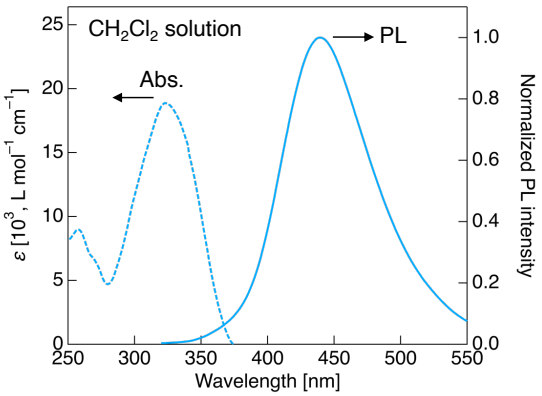

(e) **1e**

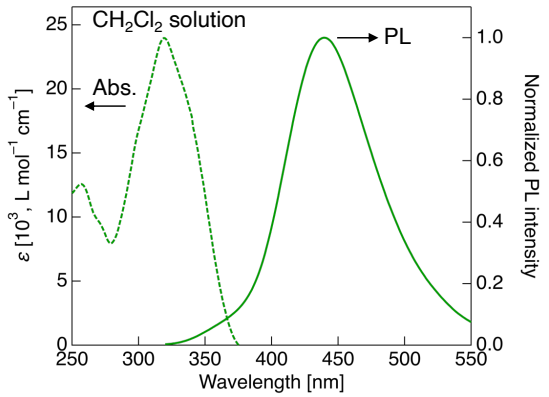

(f) **1f**

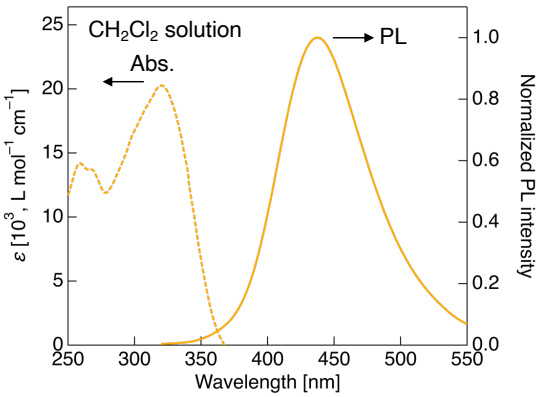

(g) **1g**

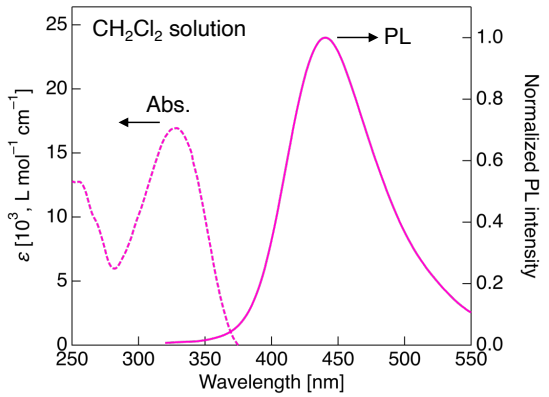

(h) **1h**

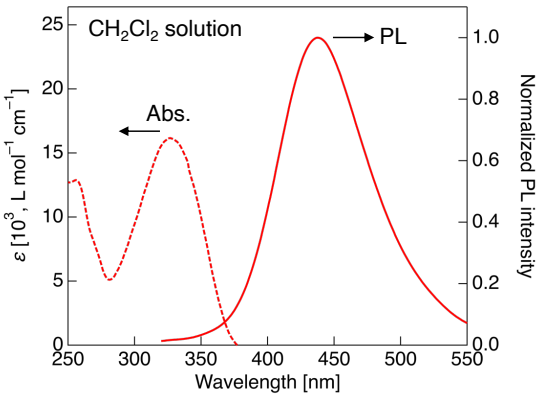

Figure S28. UV-vis absorption and PL spectrum of **1a**–**h** in CH_2Cl_2 solution (1.0×10^{-5} mol L^{-1}).

Solvatochromic PL behavior

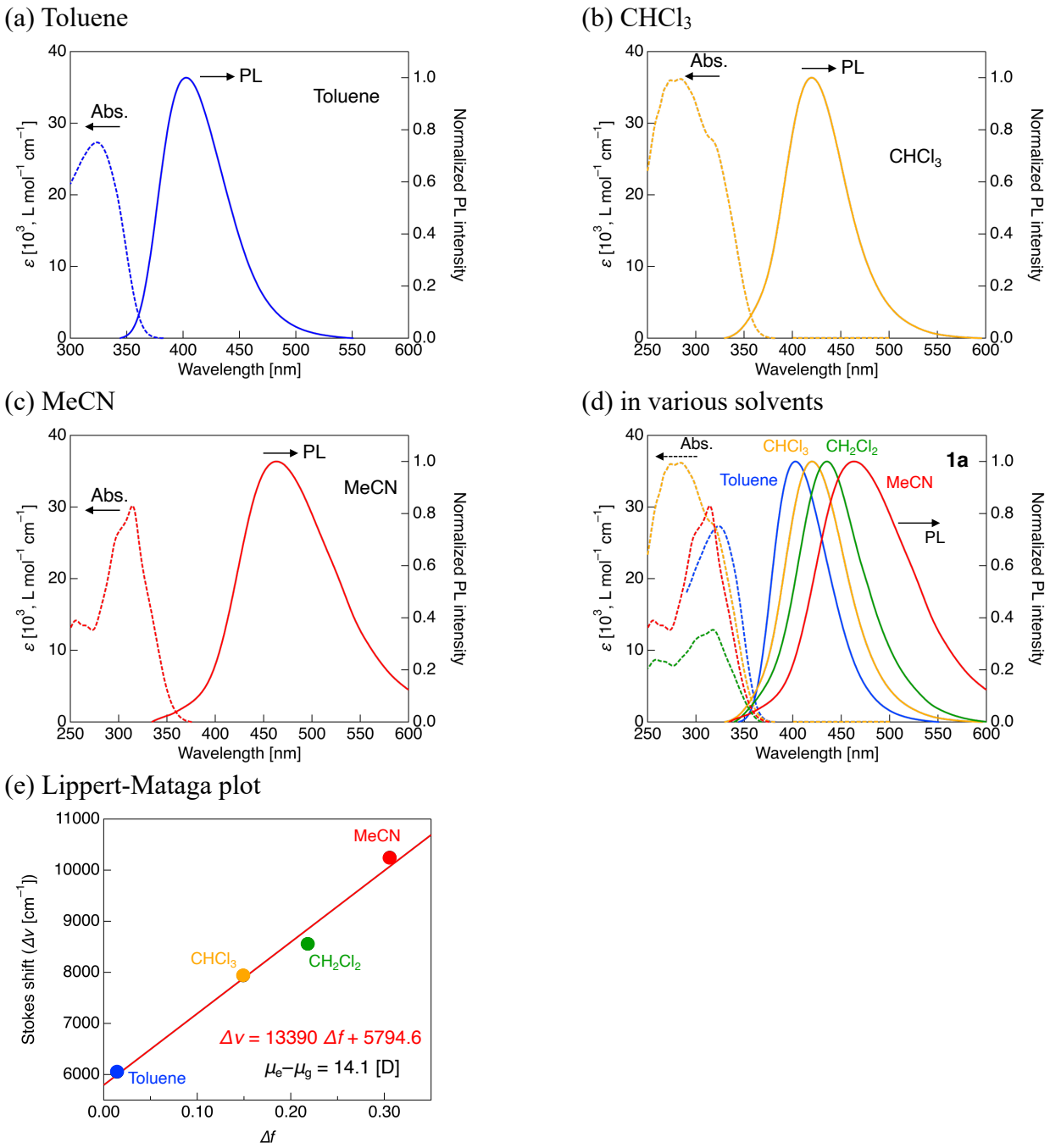

Figure S29. UV-vis absorption and PL spectra of **1a** in a different solvent: (a) toluene, (b) $CHCl_3$, (c) MeCN. (d) in various solvents, (e) Lippert-Mataga plot of **1a**.

Table S3. Solvent effect on the photophysical behavior.

	ε (25 °C)	n	Δf	ν_{Abs}	ν_F	$\Delta\nu$
Toluene	2.3807	1.494	0.01416715	30864	24814	6050
$CHCl_3$	4.806	1.443	0.14909508	31746	23810	7936
CH_2Cl_2	8.93	1.421	0.21817531	31546	22989	8557
MeCN	35.94	1.341	0.30574908	31847	21598	10249

Cry phase

(a) **1a**

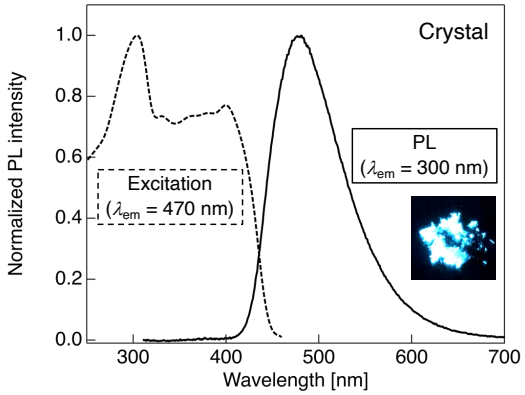

(b) **1b**

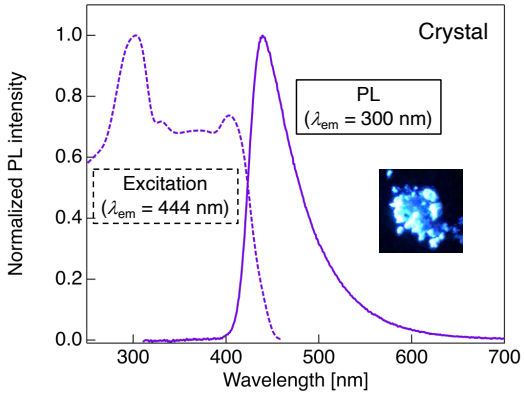

(c) **1c**

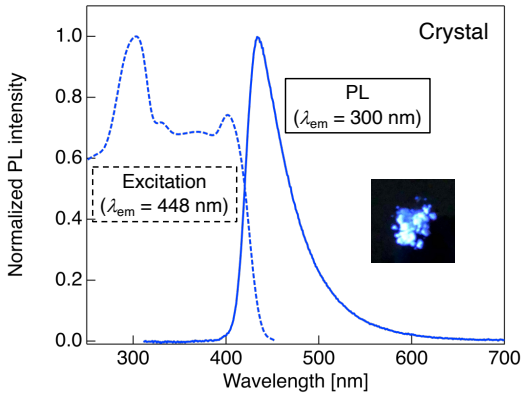

(d) **1d**

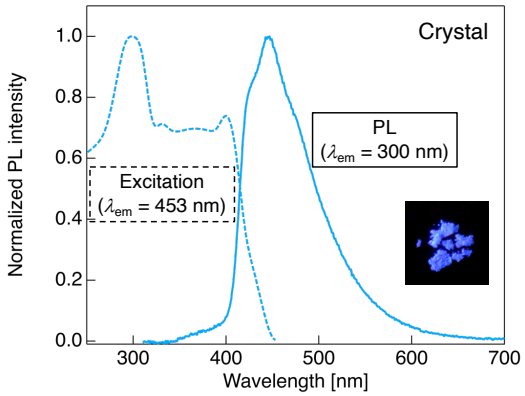

(e) **1e**

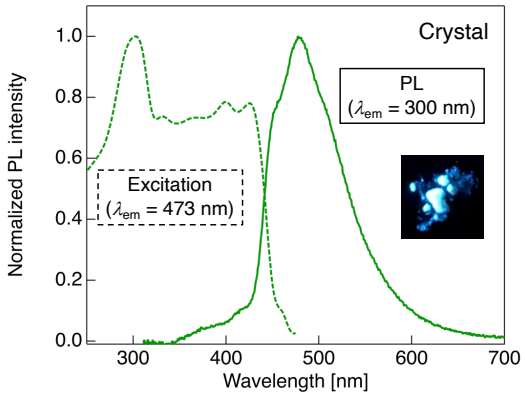

(f) **1f**

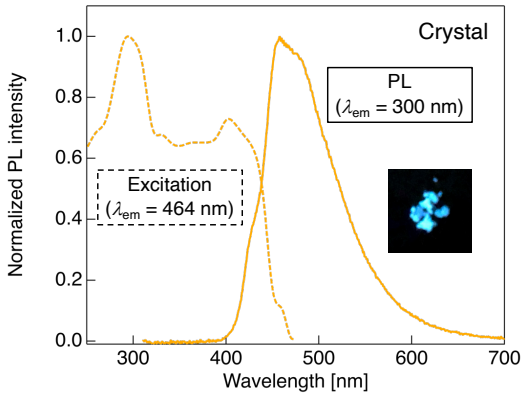

(g) **1g**

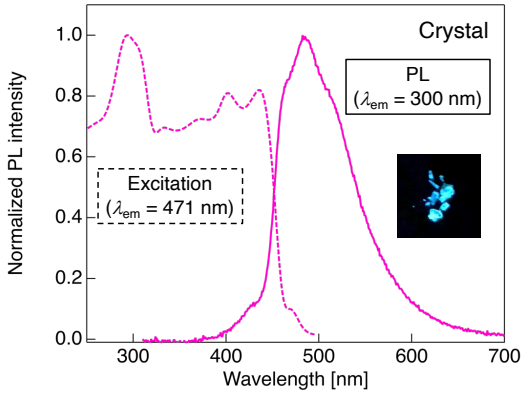

(h) **1h**

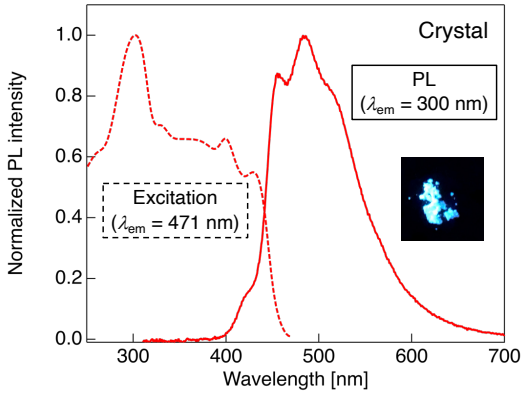

Figure S30. Excitation and PL spectra of **1a**–**h** in Cry phase.

Nematic LC phase

(a) (b)

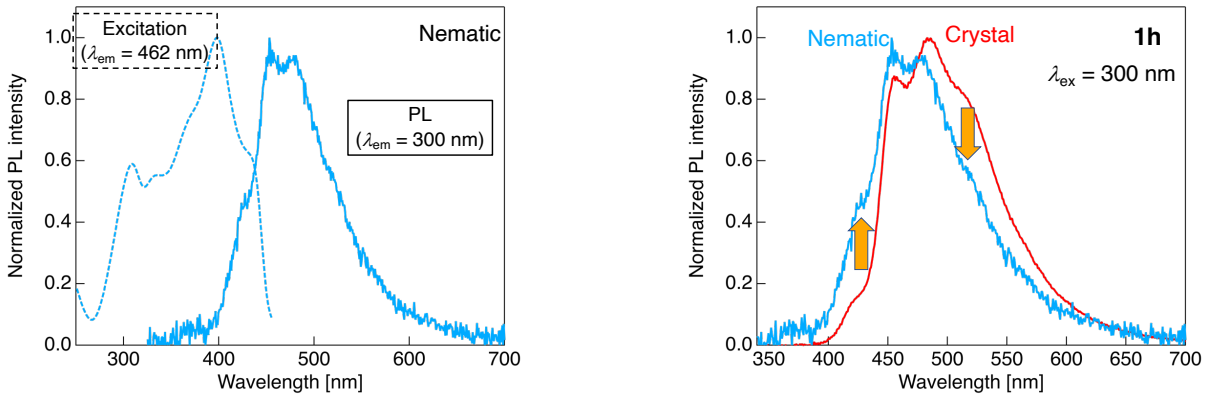

Figure S31. (a) Excitation and PL spectrum of **1h** in the aggregated structure of nematic phase. (b) Difference in PL spectrum between Cry and N phases.

Quantum chemical calculation

Quantum chemical calculation was performed using the Gaussian 16 program set. The initial structure for quantum chemical calculations was optimized by the structural optimization calculation with the M06-2X functional and the 6-31+G(d,p) basis set. Theoretical vertical electronic transitions were determined by time-dependent self-consistent field (TD-SCF) approximation.

(a) Optimized structure

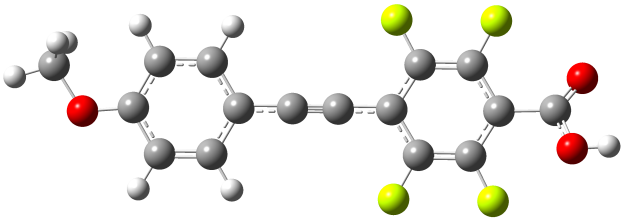

(b) HOMO–1 (–8.84 eV)

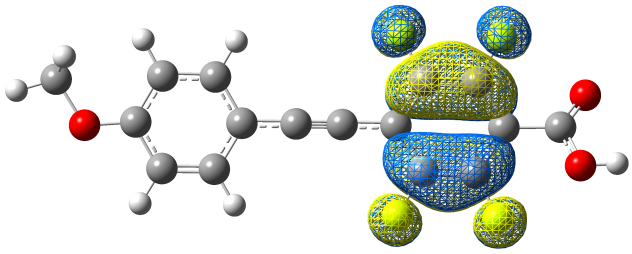

(c) HOMO (–7.45 eV)

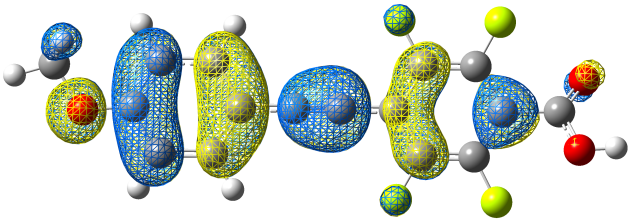

(d) LUMO (–1.75 eV)

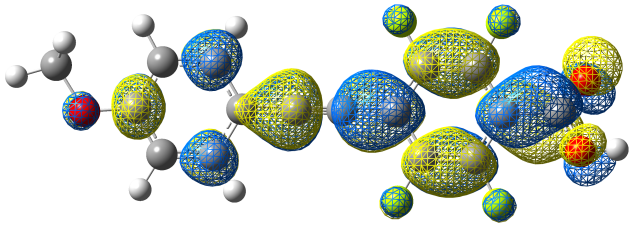

(e) Theoretical data

<Optimization>

SCF Done: E(RM062X) = –1239.07820687 Hartree A.U. after 10 cycles

Dipole moment (field-independent basis, Debye):

X= 4.6107 Y= 0.0184 Z= –1.0269 Tot= 4.7237

<TD-SCF>

Excited State 1: Singlet-A 3.8827 eV 319.33 nm f=1.3882 <S**2>=0.000

79 → 83 0.11368

82(H) → 83(L) 0.67893

This state for optimization and/or second-order correction.

Total Energy, E(TD-HF/TD-DFT) = -1238.93552070

Copying the excited state density for this state as the 1-particle RhoCI density.

Excited State 2: Singlet-A 4.6453 eV 266.90 nm f=0.0644 <S**2>=0.000

79 → 87 0.14571

81(H–1) → 83(L) 0.65560

82 → 87 0.16620

Figure S32. (a) Optimized structure of **1a** and its orbital distributions for (b) HOMO–1, (c) HOMO, and (d) LUMO. (e) Theoretical data calculated by optimization and TD-SCF calculation.

(a) Optimized structure

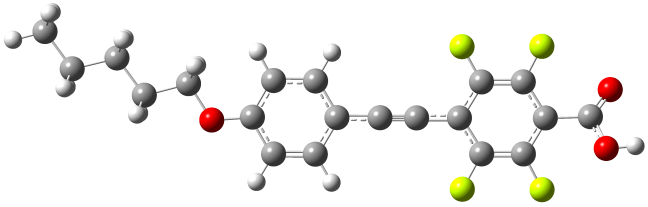

(b) HOMO–1 (–8.84 eV)

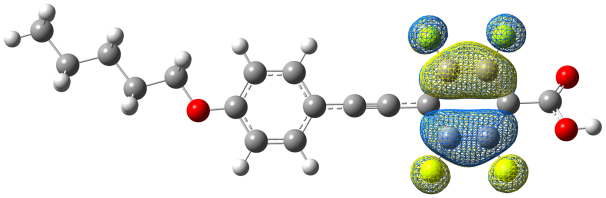

(c) HOMO (–7.44 eV)

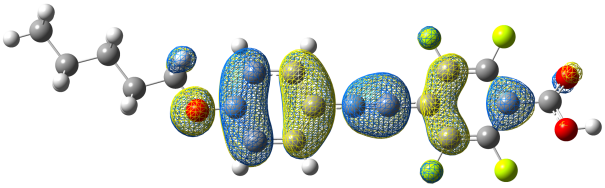

(d) LUMO (–1.75 eV)

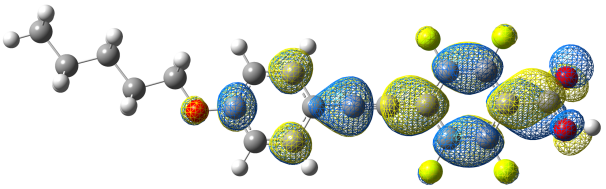

(e) Theoretical data

<Optimization>

SCF Done: E(RM062X) = –1396.26476274 Hartree A.U. after 11 cycles

Dipole moment (field-independent basis, Debye):

X= –5.0394 Y= –0.3780 Z= 0.9308 Tot= 5.1385

<TD-SCF>

Excited State 1: Singlet-A 3.7717 eV 328.73 nm f=1.5811 <S**2>=0.000

95 → 99 -0.12014

98(H) → 99(L) 0.67727

This state for optimization and/or second-order correction.

Total Energy, E(TD-HF/TD-DFT) = -1396.12615684

Copying the excited state density for this state as the 1-particle RhoCI density.

Excited State 2: Singlet-A 4.6185 eV 268.45 nm f=0.0897 <S**2>=0.000

95 →103 0.13470

97(H–1) → 99(L) 0.66107

98 →103 -0.15373

Figure S33. (a) Optimized structure of **1e** and its orbital distributions for (b) HOMO–1, (c) HOMO, and (d) LUMO. (e) Theoretical data calculated by optimization and TD-SCF calculation.

Table S4. Cartesian coordinate for **1a**.

No.	Atom No.	Type	Coordinates (Angstroms) x	y	z
1	8	0	7.119914	-0.378629	0.015764
2	6	0	5.775929	-0.230893	0.008445
3	6	0	5.121218	1.003920	-0.068737
4	1	0	5.676208	1.931716	-0.129124
5	6	0	3.730007	1.041741	-0.068187
6	1	0	3.220313	1.997825	-0.127723
7	6	0	2.978192	-0.137572	0.007627
8	6	0	3.649655	-1.373275	0.084078
9	1	0	3.075449	-2.291986	0.143189
10	6	0	5.031173	-1.418495	0.084775
11	1	0	5.561379	-2.362943	0.143874
12	6	0	1.551074	-0.089010	0.007713
13	6	0	0.338712	-0.050904	0.008275
14	6	0	-1.080599	-0.011156	0.008293
15	6	0	-1.781305	1.198748	-0.013885
16	6	0	-3.164992	1.235515	-0.005529
17	6	0	-3.925545	0.063407	0.008872
18	6	0	-3.228813	-1.147279	0.024796
19	6	0	-1.844563	-1.181829	0.031048
20	9	0	-1.108028	2.349768	-0.046825
21	9	0	-3.753003	2.430068	-0.046816
22	9	0	-3.873721	-2.313079	0.069227
23	9	0	-1.232809	-2.366883	0.064482
24	6	0	-5.417349	0.146047	0.034096
25	8	0	-5.994684	-0.876323	-0.598847
26	8	0	-6.028067	1.044897	0.560405
27	1	0	-6.958948	-0.772991	-0.532548
28	6	0	7.922526	0.792457	-0.059149
29	1	0	8.954696	0.448067	-0.037302
30	1	0	7.734698	1.334591	-0.991283
31	1	0	7.735042	1.448763	0.796563

Table S5. Cartesian coordinate for **1e**.

No.	Atom No.	Type	Coordinates (Angstroms) x	y	z
1	8	0	-5.233268	-0.983555	-0.008581
2	6	0	-3.902604	-0.745975	-0.008320
3	6	0	-3.331962	0.532708	0.004708
4	1	0	-3.948396	1.422687	0.015511
5	6	0	-1.946680	0.664341	0.003831
6	1	0	-1.502746	1.654443	0.013921
7	6	0	-1.116417	-0.463791	-0.009976
8	6	0	-1.702733	-1.744165	-0.023071
9	1	0	-1.067721	-2.623880	-0.033705
10	6	0	-3.078150	-1.882536	-0.022219
11	1	0	-3.542977	-2.862578	-0.032097
12	6	0	0.303959	-0.317835	-0.010398
13	6	0	1.510726	-0.194876	-0.010593
14	6	0	2.922726	-0.045697	-0.009669
15	6	0	3.524969	1.215884	0.024526
16	6	0	4.901259	1.362937	0.018146
17	6	0	5.752622	0.255129	-0.006810
18	6	0	5.154552	-1.006935	-0.035423
19	6	0	3.777374	-1.151703	-0.043126
20	9	0	2.762230	2.309320	0.068483
21	9	0	5.392150	2.600109	0.072594
22	9	0	5.890712	-2.116862	-0.092038
23	9	0	3.261753	-2.381238	-0.089416
24	6	0	7.233299	0.455578	-0.029042
25	8	0	7.888700	-0.520543	0.600679
26	8	0	7.772067	1.402214	-0.550215
27	1	0	8.841756	-0.340782	0.536138
28	6	0	-6.124062	0.132049	0.005280
29	1	0	-5.938293	0.736128	0.903137
30	1	0	-5.941128	0.755990	-0.879490
31	6	0	-7.541874	-0.403214	0.001478
32	1	0	-7.683306	-1.028491	-0.888146
33	1	0	-7.681200	-1.047095	0.878068
34	6	0	-8.571119	0.725976	0.014566
35	1	0	-8.417268	1.373825	-0.859242
36	1	0	-8.415469	1.355217	0.901547
37	6	0	-10.009892	0.211462	0.010578
38	1	0	-10.163943	-0.417849	-0.874986
39	1	0	-10.162434	-0.435915	0.883293
40	6	0	-11.034755	1.343638	0.023096
41	1	0	-10.914713	1.986918	-0.854947
42	1	0	-12.057953	0.957893	0.020008
43	1	0	-10.913225	1.968767	0.913952